Axial capacity of back-to-back built-up aluminum alloy channel section columns

Roy, Krishanu; Chen, Boshan; Fang, Zhiyuan; Uzzaman, Asraf; Lim, James B. P.

Published in:
Journal of Structural Engineering (ASCE)

DOI:
10.1061/(asce)st.1943-541x.0003238

Published: 28/02/2022

Document Version
Peer reviewed version

Axial capacity of back-to-back built-up aluminium alloy channel section columns

Krishanu Roy[1,*], Boshan Chen[2], Zhiyuan Fang[3], Asraf Uzzaman[4], James B.P. Lim[5]

[1] Lecturer, Dept. of Civil and Environmental Engineering, Univ. of Auckland, Auckland, New Zealand. ORCID: https://orcid.org/0000-0002-8086-3070. Email: kroy405@aucklanduni.ac.nz

[2] Ph.D. Student, Dept. of Civil and Environmental Engineering, Univ. of Auckland, Auckland, New Zealand. ORCID: https://orcid.org/ /0000-0001-9176-0731. Email: bche719@aucklanduni.ac.nz

[3] Ph.D. Student, Dept. of Civil and Environmental Engineering, Univ. of Auckland, Auckland, New Zealand. ORCID: https://orcid.org/0000-0003-1186-5221. Email: zfan995@aucklanduni.ac.nz

[4] Lecturer, School of Computing, Engineering and Physical Sciences, University of the West of Scotland, Paisley, PA1 2BE, United Kingdom Asraf.Uzzaman@uws.ac.uk

[5] Associate Professor, Dept. of Civil and Environmental Engineering, Univ. of Auckland, Auckland, New Zealand. ORCID: https://orcid.org/0000-0001-9720-8518. Email: james.lim@auckland.ac.nz

*Corresponding Author Contact Details:

Krishanu Roy

E: krishanu.roy@auckland.ac.nz, T: +64 223917991, F: +64 9 373 7462, Department of Civil Engineering, University of Auckland, Auckland, New-Zealand-1025

Abstract

An experimental investigation of 12 screw fastened back-to-back built-up aluminium alloy slender columns under axial compression is presented, complemented by a numerical finite element study comprising 246 results. Using a laser scanner, the geometric imperfections were measured. In the numerical study, the effect of the modified slenderness, number of screws and section thickness were investigated. Axial strengths obtained from the tests and FE were used to assess guidance given in the Aluminium Design Manual (ADM 2020), Eurocode9 (CEN 2007), Australian/New Zealand Standards (AS/NZS 2018), and American Iron and Steel Institute (AISI 2016) standards. The ADM 2020 and CEN 2007 were found to be conservative by 30%. However, AISI 2016 & AS/NZS 2018 were found to be more accurate relative to the test and FEA results and shown to be conservative by 5%.

Keywords

Aluminium alloy, slender columns, finite element analysis, axial compression tests, built-up sections

1 Introduction

As aluminium alloy becomes more popular in the building industry (Miller et al. 2000; Roy et al. 2021; International Aluminium Institute 2011), the uses of such back-to-back built-up sections as the primary load bearing column members are increasing. This paper considers the axial strength of such sections and 12 new experimental tests and 246 finite element (FE) analysis results are presented. Fig.1 shows the details of the built-up columns investigated in this study. A photograph of the built-up section prior to compression test is shown in Fig.2, where the general arrangement of the intermediate screw fasteners between the back-to-back channels are shown.

The Aluminium Design Manual (ADM 2020) and Eurocode 9 (CEN 2007) both provide recommendations for designing the aluminium alloy single channel section columns under axial load. However, they do not include recommendations for such back-to-back built-up aluminium alloy channel sections. The American Iron and Steel Institute (AISI 2016) and Australian and New Zealand Standards (AS/NZS 2018) both recommend the same modified slenderness approach to take into account spacing of screws in built-up columns. However, this approach is for cold-formed steel (CFS) members instead of aluminium alloy members. In the literature, no papers have been reported addressing this issue.

For cold-formed carbon steel, however, research has been reported. Ting et al. (2018) investigated the effect of screw-spacing on axial strength of back-to-back built-up CFS channel sections (Fig.3). Roy et al's (2018a,b) investigated the effect of a gap (Fig.4). Crisan et al. (2014) presented the results of numerical models, where the sections were built up through battens. Rondal and Niazi (1990) described laboratory tests for built-up CFS columns, connected with spacers. Dabon et al. (2015a,b) studied the behaviour and design of CFS battened built-up columns. Recently, Roy at el. (2018c) investigated the effect of section thickness. Fratamico et al. (2018) studied the collapse of back-to-back built-up CFS lipped channel section columns. For un-lipped channels, Roy et al. (2019) investigated the effect of screw spacing, concluding that AISI 2016 & AS/NZS 2018 can be un-conservative for built-up columns, where failure is through local buckling. Finally, Kesawan et al. (2017) presented an experimental investigation on the structural performance using hollow flange I-section columns.

At the same time, stainless steel built-up columns are also becoming increasingly popular; they are aesthetic, possess corrosion resistance and are therefore easy to maintain, and also convenient for assemblage and construction. (Young and Hartono 2002). Standards that cover stainless steel built-up columns include AS/NZS 2001, AISI 2016 and ASCE 2002; it should be noted though that the design guidance is not specific to the grade. In terms of recent studies, Yuan et al. (2014) presented the results of experimental tests on stainless steel back-to-back built-up sections under axial compression. Roy et al. (2018d, 2019b,c,d) and Dobric et al. (2018a,b) considered the behaviour of different cross-sections under axial compression. Finally, Kechidi et al. (2017,2020) investigated the screws spacings and their effect on axial strength

As mentioned previously, however, for aluminium alloy single channel section columns, research reported in the literature is limited. Feng et al. (2015,2016,2017) and Chen et al. (2017,2018) investigated the effect of perforations on such single channel sections used as columns; these included columns, square hollow section members, circular hollow section tubes, and square and rectangular sections. From this work it was found that current design rules (CEN 2007) were not appropriate for determining their strength under compression. Furthermore, Huynh et al. (2016a,b, 2020) conducted experiments to study the buckling behaviour of aluminium alloy channel sections. For the case of aluminium alloy angle sections, Mazzolani et al. (2000,2011) investigated the effects of width-to-thickness ratio and the occurrence of local buckling for such sections under axial compression. Su et al. (2013,2014,2016) has developed a Continuous Strength Method (CSM) to study the compression resistance of aluminium alloy column members.

2 Experimental Study

2.1 Test specimens

Under axial compression, 12 successive aluminium alloy built-up channel sections were tested to failure in this study. Nominal cross-sections of test specimens considered in this study are shown in Fig.2: BU150×65×25 and BU240×45×20. It should be mentioned that the material grades of aluminium alloy channel sections utilised in this study are 5052-H32 for section BU2404520 and 5050-H32 for section BU1506525, respectively. In terms of cross-section categorization, it should be emphasised that the cross-sections employed in this study are classified as Class 4. The dimensions of test specimens are shown in Table 1. Test specimens were subdivided into two different column lengths: intermediate (1000mm) and slender (1500mm). According to the requirements of AISI 2016 and AS/NZS 2018, the following longitudinal screw spacings (S) were considered:

- Column length of 1000mm; screw spacings of 225mm, 450mm and 900mm
- Column length of 1500mm; screw spacings of 350mm, 700mm and 1400mm

2.2 Section labels

The test specimens were labelled to show the web depth, longitudinal spacing between fasteners, nominal length of section, and specimen number (Fig.5). For instance, the designation "BU150-S225-L1500" has been read as follows:

- 150 denotes the depth of web in millimetres i.e. *d* =150mm;
- “L1500” denotes the length of the specimen in millimetres;
- “S225” denotes the screw spacing in millimetres.

2.3 Material testing

To assess the material properties of test specimens, tensile coupon tests were performed. Coupons were cut in the longitudinal directions of untested specimens from the centre of the web plate, in line with the British Standard for Testing and Materials (BS EN 2001). Table 2 details the size of the coupons. The coupons were tested using a 50 kN capacity Instron tensile testing machine. The coupons' tensile strain was determined using a calibrated extensometer with a gauge length of 50mm. Fig.6 depicts the complete stress–strain curves for BU1506525 and BU2404520. Table 3 summarises the material properties derived from the tensile coupon testing. The yield strengths of BU1506525 and BU2404520 are, on average, 108.40MPa and 150.50MPa, respectively, as shown in Table 3. Serrated yielding was seen in the coupon tests, and serrations occurred after achieving the 0.2% proof stress, as illustrated in Figs 6(b,d). Huynh et al. also observed this phenomena (2019).

2.4 Test-rig and loading process

The axial load was applied to the aluminium alloy built-up columns using a universal testing equipment with a capacity of 500 kN. The load was delivered through the specimens' centres of gravity (CG) in pin-ended boundary conditions. It is worth noting that the pin support utilised in this investigation was a shaft passing through a bearing. To verify that no space existed between specimens' two pin-ends and end plates, all columns were initially loaded to 25% of their predicted failure load and then released. Fig.7 illustrates the test configuration for intermediate column testing. Fig.8 depicts the pin support that was utilised in the test configuration. In the column testing, displacement control was employed to produce the load at a steady rate of 0.02mm/s.

At the top of the built-up columns, an external load cell was installed. The displacements were recorded using a total of three linear variable differential transformers (LVDTs). The axial shortening of specimens was determined using LVDT-1 data, and the lateral displacements were determined using LVDT-2 and LVDT-4 readings at one-fourth the height of the columns. Similarly, displacements at mid-height of built-up aluminium alloy channel sections were recorded using LVDT-3 and LVDT-5. Four distinct strain gauges (SG1, SG2, SG3, and SG4) were utilised to determine the strain values in the aluminium alloy built-up channel sections at mid-height (See Fig.9).

2.5 Measurements of initial geometric imperfections

All test specimens had their initial imperfections determined using a movable laser scanner, as depicted in Fig.10. A precise shaft led the laser scanner into the measurement platform in the transverse (2500mm) direction. As illustrated in Fig.11, the scanner detected initial geometric imperfections along six longitudinal lines running through aluminium alloy sections.

As shown in Fig.12(a), the calculation of the local imperfections was completed by subtracting the average readings along the W-1 and W-3 lines from the W-2 lines. As seen in Fig.12(b), the global imperfections were calculated by averaging the measurements of the line W-2 at mid-height of the columns. Meanwhile, as shown in Fig.12(c), the maximum readings on the F-1 and F-2 lines were utilised to determine the distortional imperfections.

As illustrated in Fig.12, a typical imperfection profile of BU240-S350-L1500 is plotted against the length. Table 4 summarises the degree of local, distortional, and global imperfections present in all test specimens. These values of initial geometric imperfections were used in the FE modelling described in section 3.5 of this paper. Ye et al. (2018a,b), Chen et al. (2019), Roy et al. 2019c,d,e,2020 and Chi et al. (2021) employed a similar technique to determine the initial geometric imperfections of CFS channels.

2.6 Experimental results

The column dimensions and experimental failure loads (P_{EXP}) for each test specimen are summarised in Table 1. As shown in Table 1, both BU150 and BU240 were evaluated using two groups of lengths, 1000 mm and 1500 mm. Table 1(a) demonstrates that for BU150, all intermediate and slender columns failed due to local and distortional buckling. Fig.13 plots the axial load versus lateral displacement graphs at the end and mid-height of the sections BU150-S1400-L1500 and BU240-S900-L1000, respectively. Fig.14 shows the deformed shapes of the 1000 mm and 1500mm-long BU150 and BU240 columns.

Fig.15 illustrates the load-axial shortening behaviour of intermediate and slender columns. The load-axial shortening behaviour was found to be linear up to a load of 77.95 kN, which is approximately 74.11% of the ultimate failure load for BU240-S225-L1000. Following then, nonlinear behaviour was observed until the failure load, 105.18 kN, was reached. Similar observations were found for other built-up aluminium alloy channel columns.

Four strain gauges, two in tension and two in compression, were utilised to determine the axial strain at mid-length from both ends of built-up aluminium alloy channel sections. Fig.16 depicts the load-axial strain relationship for BU240-S1400-L1500. Strain values were measured and displayed in Fig.16 at the midpoint of the built-up columns.

The influence of screw spacing on axial strength was explored and is illustrated in Table 1 and Fig.17. As illustrated in Fig.17(a), increasing the screw spacing from 225mm to 450mm, decreased the axial strength by an average of 2.62% for intermediate columns. For slender columns, doubling the screw spacing from 450mm to 900mm resulted in a 9.15% decrease in axial strength. As shown in Fig.17(b), when the screw spacing of slender columns was increased from 350 to 700mm, the average strength rose by 2.64%. A 5.86% decrease in axial strength was reported when screw spacing was increased from 700mm to 1400mm.

The specimen BU150 with lengths of 1000mm and 1500mm, failed due to localised and distortional buckling. The BU240 section, with 1000mm and 1500mm column lengths, failed primarily due to distortional and global buckling. The built-up aluminium alloy channel sections remained intact at failure, exhibiting some plastic deformation around the bottom or top of the columns. Local and distortional buckling were detected for the majority of BU150 columns. When the ultimate load was reached, localised deformation near the compression side of the columns became apparent. Fig.18 illustrates the distorted shapes of intermediate and slender columns of built-up aluminium alloy channel sections.

3 Numerical Study

3.1 General

The general purpose finite element program ABAQUS 2014 was used for the purpose of this study. Fig.19(a) shows details of a typical mesh for BU150-S225-L1000. S4R shell elements were used with a mesh size of 5mm × 5mm for the channel-sections and end plates, the mesh size determined from the results of a sensitivity study. Interactions between the webs of the channel-sections were modelled using “Surface to surface” contact. The normal behaviour of the surface was defined as “hard”. Both an elastic buckling analysis and a nonlinear static RIKS analysis were undertaken.

The true material curve was calculated from the engineering material curve from:

$$\sigma_{true} = \sigma(1+\varepsilon) \quad (1)$$

$$\varepsilon_{true(pl)} = \ln(1+\varepsilon) - \frac{\sigma_{true}}{E} \quad (2)$$

Where, E is the Young’s modulus, σ_{true} and $\varepsilon_{true(pl)}$ are the true stress and true plastic strain, respectively.

σ and ε are the engineering stress and strain, respectively.

3.2 Boundary conditions and loading procedure

Fig.19(a) shows the pin-pin boundary conditions applied for BU150-225-L1000. In the x- and y-directions the nodes were restrained; in the z direction no nodes were restrained apart from at the loading point (or reference point in ABAQUS). For the reaction point, the nodes were restrained in the x, y and z directions. In ABAQUS, the multi-point constraint (MPC) beam connector element was used such that the stiffness of the fasteners could be defined, calculated based on the screw diameter and section thickness. Using these connector element stresses, a reasonable match between the test and FEA results was achieved, therefore putting further confidence on the connector modeling technique.

3.3 Modelling of initial geometric imperfections

Geometrical Imperfections as a result of the manufacturing and transportation need to be included in the finite element model. Shapes of imperfections were obtained from eigenvalue analysis for local and global buckling and superimposed. Fig.19(b) shows the shapes of local and global buckling modes. These were performed with very small to large profile thickness to determine the contours of the geometrical imperfections (Dabaon et al. 2015b, Roy et al. 2019c,d,e,2020, Young et al. 2005, 2007). The magnitudes of the imperfections were scaled to the measured values, as shown in Table 4.

3.4 Validation of the FE model

Table 1 shows for BU150 and BU240 the comparison of the axial strengths obtained from the tests and the FEA. As can be seen, the FEA results were close to the experimental test results in terms of both axial strength and mode of failure. Fig.18 shows that the deflected shapes predicted by the FEA, for intermediate and slender columns, show good agreement with the experimental failure modes. Fig.20 plots load-axial shortening behaviour from both the FEA and experiments, again shown for the intermediate and the slender columns. The differences between the FE model prediction and the test results are again seen to be small, with the mean value of the ratio of P_{EXP}/P_{FEA} being 1.04 (COV of 0.05). Table 1 shows that the FEA strengths are slightly conservative to the experimental strengths for all experimental tests, perhaps attributed to the friction between the base plates and the edges of back-to-back built-up aluminium alloy channel sections. In the tests, the friction between the end plates and channels would normally change and it is very hard to determine the exact friction value from each of the experimental tests. As can be seen from some of the experimental failure modes, there are some localised deformations between the end plates and channels. However, in the FEA, a fixed value of coefficient of friction was set as 0.5 for all the models, based on the calibration of the FEA model and comparisons against the test results using different friction coefficients. Load versus lateral displacement curves are shown in Fig.13 for BU150-S1400-L1500 and BU240-S900-L1000, which showed good comparisons between the FEA and test results. The axial load versus axial strain relationship from both the FEA and experiments are shown in Fig.16 for BU240-S1400-L1500. As shown in Fig.16, there was reasonably good agreement between the FEA and experimentally measured strain values at mid-height of the built-up columns. Overall, the FE model showed very good correlations with the experimental results.

4 Parametric study

4.1 General

The influence of screw spacing was explored using the results of 234 FE models: covering a range of columns having different slenderness values. As shown in Table 5, column lengths from 1000mm to 3000mm and three different screw numbers (3,5 and 9) were considered in the parametric study. Besides, section thickness often plays a significant role in the structural behaviour of thin-walled structural members (Roy et al.2021, Chen et al.2019, Fang et al.2021a, b, Uzzaman 2020a,b), and thus the section thickness was included in the parametric study. Fig.21 illustrates the results of the parametric investigation, demonstrating how the axial strength of BU150 and BU240 fluctuates with the number of screws and section thicknesses.

4.2 Effect of columns' modified slenderness ((KL/r)m) on axial strength

The axial strength is shown in Table 5 as a function of modified slenderness ((KL/r)m). As can be seen, when the average modified slenderness ((KL/r)m) was increased from 14.25 to 44.77 and 17.52 to 37.91 for BU150 and BU240, respectively, the axial strengths were lowered by 6.33% and 8.09%.

4.3 Effect of screw numbers (screw spacing) on axial strength

Additionally, the influence of screw number (screw spacing) on axial strength was examined. As shown in Table 5 and Fig.21(a), increasing the screw numbers, the axial strengths of BU150 and BU240 increased by only 0.96% and 0.84%, respectively. This suggests that screw numbers (screw spacing) have negligible effects on the axial strength of such columns.

4.4 Effect of channel thickness (t) on axial strength

Table 5 and Fig.21(b) illustrate the effect of thickness on axial strength. For example, when the thickness of BU150 was increased from 1.6mm to 2.6mm, the axial strength improved by 109.37% (on average). The increase in section thickness from 1.9mm to 2.9mm showed an increase in axial strength by 99.80% (on average) for BU240.

5 Design rules for axial strength of aluminium alloy built-up sections

Current design standards, notably ADM 2020 and CEN 2007, have procedures for calculating the axial strengths of aluminium alloy single channel section columns. However, these standards contain no design requirements for determining the axial strength of built-up aluminium alloy sections. As a result, in addition to the design rules for aluminium alloy single channel section columns under compression, this study utilised the design procedures specified in AISI 2016 & AS/NZS 2018 for carbon steel built-up columns.

5.1 Design rules for aluminium alloy single channel section columns

The design strengths of aluminium alloy single channel section columns can be estimated using the Aluminium Design Manual (ADM 2020) and Eurocode 9 as design guidelines (CEN 2007). As previously stated, these guidelines are applicable only to the design of aluminium alloy single channel section columns. As a result, the design calculation projected that built-up aluminium alloy channel sections would be twice as strong as single channel sections. Additionally, to account for the effects of screw fastener spacing between aluminium channels, the modified slenderness ratio ((KL/r)m) specified in the cold-formed steel design standards (AISI 2016 & AS/NZS 2018) was calculated for the aluminium built-up sections and then substituted into the ADM 2020 and CEN 2007 design equations. All dimensions and material properties used in the design calculations were taken from the experimental values.

5.1.1 Aluminium design manual (ADM 2020)

In accordance with the ADM 2020, axial strength (P_{ADM})of aluminium alloy single channel section columns can be determined by using Equation (3):

$$P_{\mathrm{ADM}} = \min(P_{n1}, P_{n2}, P_{n3}) \tag{3}$$

The design compressive strength ($\phi_c P_{n1}$) as well as the allowable compressive strength (P_{n1}/Ω_c) within the aluminium design manual (P_{ADM}) employ the lowest of the strengths for the limit states of member buckling (P_{n1}), local buckling (P_{n2}), as well as the interaction among both member and local buckling (P_{n3}).

The member buckling strength (P_{n1}) is available in chapter E.2 of ADM 2020 as:

$$P_{n1} = f_c A_g \tag{4}$$

Where,

$$f_c = \begin{cases} f_y & \lambda \le \lambda_1 \\ 0.85(B_c - D_c\lambda) & \lambda_1 < \lambda \le \lambda_2 \\ \dfrac{0.85\pi^2 E}{\lambda^2} & \lambda \ge \lambda_2 \end{cases} \tag{5}$$

The weighted average local buckling strength (P_{n2}) was calculated in accordance with Chapter E.4.1 of ADM 2020 as follows:

$$P_{n2} = \sum_{i=1}^{n} f_{ci}A_i + f_{cy}(A_g - \sum_{i=1}^{n} A_i) \quad (6)$$

The strength of interaction between the member buckling and local buckling (P_{n3}) was determined as per the design rules given in chapter E.5 of ADM 2020 as given next.

$$P_{n3} = [\frac{0.85\pi^2 E}{\lambda^2}]^{1/3} f_e^{2/3} A_g \quad (7)$$

where, A_g represents the gross cross-sectional area; A_i represents the area of each element (marked as *i*); B_c represents the buckling constant intercept for axial compression in flat element in Table B4.1 of the ADM 2020; C_c represents the buckling constant intersection for compression in columns and beam flanges in Table B4.1 of the ADM 2020; D_c represents the buckling constant slope for compression in columns and beam flanges as in Table B4.1 of the ADM 2020; f_c represents the stress of the uniform compressive strength; f_{ci} represents the local buckling stress for every element (marked as *i*); f_e represents the elastic buckling stress computed in Table B5.1 of the ADM 2020; λ represents the largest column modified slenderness from Sections E3.1 and E3.2 of the ADM 2020; $\lambda_1=(B_c-f_{cy})/D_c$, represents the slenderness for the intersection of yielding and inelastic buckling; f_{cy} represents the compressive yield strength; and finally, $\lambda_1=C_c$, represents the slenderness for the intersection of inelastic and elastic buckling.

5.1.2 Eurocode 9 (CEN 2007)

In accordance with the Eurocode 9(CEN 2007), the design axial strength (P_{EN}) of aluminium alloy single channel section columns can be determined as follows:

$$P_{EN} = \kappa\chi A_{eff} f_o / \gamma_{M1} \quad (8)$$

Where, A_{eff} represents the effective section area as per the reduced thickness allowing for local buckling, and it is equal to the gross section area of the column; κ represents the factor for the allowed weakening effects, the value of which is set as 1; χ represents the reduction factor for the relevant buckling mode; f_0 represents the characteristic value of 0.2% of the tensile proof stress ($\sigma_{0.2}$); γ_{M1} represents the partial safety factor that was set as 1.1.

5.2 Design rules for back-to-back built-up CFS channel section columns

The un-factored design strengths of the cold-formed carbon steel built-up columns according to the AISI 2016 and AS/NZS 2018 can be computed using Equations (9)-(10).

$$P_{AISI\,\&\,AS/NZS} = A_g F_n \tag{9}$$

The critical elastic buckling stress (F_n) was computed using Equations (10)-(11).

$$F_n = \begin{cases} (0.658^{\lambda_c^2})F_y & \lambda_c \le 1.5 \\ \left(\dfrac{0.877}{\lambda_c^2}\right)F_y & \lambda_c \succ 1.5 \end{cases} \tag{10}$$

Where non-dimensional critical slenderness (λ_c) was computed using Equation (11).

$$\lambda_c = \sqrt{\frac{f_y}{f_{oc}}} \tag{11}$$

Where, f_y represents the yield stress and f_{oc} represents the least of elastic flexural, torsional as well as flexural-torsional buckling stresses, computed according to C3.1.1 of the AS/NZ 2018.

Modified slenderness ratio was computed by using Equation (12):

$$\text{For } \left(\frac{a}{r_i}\right) \le 0.5\left(\frac{KL}{r}\right)_o, \quad \left(\frac{KL}{r}\right)_m = \sqrt{\left(\frac{KL}{r}\right)_o^2 + \left(\frac{a}{r_i}\right)^2} \tag{12}$$

Where, $(KL/r)_o$ is the slenderness ratio; a represents the intermediate fastener or the spot weld spacing; and r_i represents the minimum radius of gyration of full unreduced cross-sectional area of the shape in a built-up section.

As previously mentioned, to include the effects of screw fastener spacing, the modified slenderness ratio ($(KL/r)_m$) was computed based on Equation 12 for the aluminium built-up sections, and was utilized in the design equations of the ADM 2020 as well as CEN 2007 standards.

6 Comparison of design strengths against test and FE strengths

The experimental and FEA-derived axial strengths were compared to the design values computed in compliance with ADM 2020, CEN 2007, AISI 2016, and AS/NZS 2018. Table 6 and Fig. 22(a) show the comparison results for BU150 and BU240, respectively. As can be seen, the ADM 2020 and CEN 2007 design strengths are conservative. Due to the omission of certain elements such as screw spacing and back-to-back interaction in the ADM 2020 and CEN 2007, the discrepancy between experimental and design strengths varied by approximately 30%. In accordance with AISI 2016 and AS/NZS 2018, the design strengths for BU150 and BU240 are conservative by less than 5%.

The parametric investigation was conducted using validated finite element models, with the built-up columns restrained at the end to avoid any shear deformation. The parametric study's results, as shown in Table 7, were used to compare the axial strengths of built-up columns found using FEA to the design strengths estimated in line with current ADM 2020, CEN 2007, and AS/NZS 2018. Fig.22(b) illustrates the relationship between the design strengths and the FEA results. It was discovered that the design strengths were on average 30% too conservative. The design guidelines of AISI 2016 & AS/NZS 2018 could more accurately forecast the axial strengths (Table 7), being less than 10% conservative for the majority of columns.

Figs. 22(c) and (e) plotted the BU150 and BU240 columns' test, FEA, and design strengths versus their section thickness and non-dimensional slenderness, respectively. Fig.22(d) illustrates the axial strength of columns with 3, 5, and 9 screws for BU150 and BU240. As illustrated in Fig.22 and Table 7, the FEA strengths for both BU150 and BU240 were in good agreement with the design strengths anticipated by AISI 2016 & AS/NZS 2018. Additionally, increasing the screw numbers from 3 to 9 and from 3 to 5, reduces the discrepancy between design and FEA strengths (Fig.22(d)). Fig. 22(e) demonstrates that the distortional buckling curves of AISI 2016 & AS/NZS 2018 closely match the FEA data points.

The mean P_{ADM} value for BU150 columns with 1000mm and 1500mm lengths is 1.00 and 1.03, with COVs of 0.03 and 0.01, respectively (see Table 6). In terms of BU240, the values were 1.32 and 1.17, with COVs of 0.08 and 0.05, respectively. For the intermediate and slender columns of the BU150 series, the average values of $P_{FEA}/P_{AISI\&AS/NZS}$ are 0.96 and 1.06, respectively, with COVs of 0.00 and 0.01 (Table 6(a)). The mean values of the ratio $P_{FEA}/P_{AISI\&AS/NZS}$ for BU240 are 1.08 and 0.98, with COVs of 0.05 and 0.04 (Table 6(b)). Based on the findings of parametric investigation, it can be stated that AISI 2016 & AS/NZS 2018 are more accurate at predicting the axial strengths of built-up aluminium alloy channel section intermediate and slender columns than ADM 2020. To account for the composite actions between the back-to-back channels, the modified slenderness ratio ((KL/r)m) as specified in the cold-formed steel design standards (AISI 2016 & AS/NZS 2018) was first calculated, taking into account the effect of screw spacing between the aluminium back-to-back channels, and then substituted into the design equations of ADM 2020 and CEN 2007 standards. When axial strengths of built-up columns are compared to those of single channels, it can be inferred that the axial strengths of built-up aluminium columns determined from the ADM 2020 and CEN 2007 standards utilising the modified slenderness approach were increased by approximately 5%.

The influence of screw numbers (screw spacing) on the axial strengths of built-up columns is plotted in Fig.22(d). For intermediate and slender columns, raising the screw numbers from three to nine had a negligible influence on the axial strength of built-up aluminium alloy channel section columns (less than 5%).

7 Conclusions

This article reported an experimental investigation of the axial strength of back-to-back screw connected built-up aluminium alloy channel sections when compressed axially. The findings of twelve new experiments are presented. Prior to compression tests, the material characteristics of aluminium alloy channel sections were determined using tensile coupon tests, and the initial geometric imperfections were quantified using a laser scanner. The failure modes were reported, as well as the load-axial shortening, load-lateral displacement, and load-axial strain relationships. The experimental investigation additionally examined the impacts of column modified slenderness, screw numbers (screw spacing), and section thickness.

After that, a non-linear finite element model was built that includes screw modelling, material non-linearity, and initial geometric imperfections. The results of the FE model were compared to the experimental results. This demonstrated an excellent match in terms of both axial strength and failure mechanisms. The verified finite element model was then utilised to conduct a parametric investigation using 234 models to determine the influence of changing column slenderness, screw number (screw spacing), and section thickness on the axial strength of built-up aluminium alloy channel sections. According to the parametric study's findings, section thickness can have a substantial effect on the axial strength of such columns. When the section thickness of BU150 was increased from 1.6mm to 2.6mm, the axial strength rose by an average of 109.37%. On the other hand, when the section thickness was increased from 1.9mm to 2.9mm, the axial strength was improved by 99.80% on average. However, the effect of columns' modified slenderness was not significant for intermediate and slender columns. The axial strengths of BU150 and BU240 were reduced by 6.33% and 8.09%, respectively, when the modified slenderness of the columns was increased from 14.25 to 44.77 and from 17.52 to 37.91. Screw spacing has a negligible effect on the axial strength of built-up aluminium alloy channel sections. When screw numbers were increased from three to nine, the axial strength of columns rose by just 0.96% and 0.84% (on average) for BU150 and BU240, respectively.

The experimental and FEA-derived axial strengths were compared to the design strengths computed in accordance with the Aluminium Design Manual (ADM 2020), Eurocode 9 (CEN 2007), American Iron and Steel Institute (AISI 2016) standard, and Australian/New Zealand Standard (AS/NZS 2018). ADM 2020 and CEN 2007 both apply to the construction of single channel sections made of aluminium alloy. As a result, the strength of built-up aluminium alloy channel sections was considered to be double that of a matching single channel section in the design calculations. Additionally, the axial strengths of aluminium alloy built-up sections were estimated using the design guidelines of cold-formed carbon steel as specified in AISI 2016 and AS/NZS 2018. By comparing the design strengths to the test and FEA strengths, it was determined that the design, when compliant with ADM 2020 and CEN 2007, can be conservative by around 30% on average. However, the AISI 2016 and AS/NZS 2018 standards may produce highly accurate forecasts, being only 5% conservative to the experimental and FE results on average.

To calculate the design strengths of built-up aluminium channels in accordance with ADM 2020 and CEN 2007, as well as to account for composite actions between the back-to-back channels, the modified slenderness ratio ($(KL/r)_m$) as specified in cold-formed steel design standards (AISI 2016 & AS/NZS 2018) was first calculated, taking into account the effect of screw spacing between the aluminium channels. When axial strengths of built-up columns were compared to those of single channels, it was discovered that the axial strengths of built-up aluminium columns determined from the ADM 2020 and CEN 2007 standards using the modified slenderness approach were increased by 5%. As a result, it is recommended that the axial strength of back-to-back built-up aluminium alloy channel section columns be calculated using the modified slenderness approach described in the design guidelines for cold-formed steel standard: AISI 2016 & AS/NZS 2018.

Data Availability Statement

All of the data and models generated or used during the study appear in the submitted article.

Acknowledgements

The experimental work was carried out in the “Structures test hall”, the Civil and Environmental Engineering department of University of Auckland. The help of Mark Byrami in setting up the tests is greatly appreciated.

References

ABAQUS Analysis User's Manual-Version 6.14-2. ABAQUS Inc., USA, 2014.

ADM (Aluminum Association). 2020. Aluminum Design Manual. Washington, D.C., USA, 2020.

AISI (American Iron and Steel Institute). 2007. Specifications for the coldformed steel structural members, cold-formed steel design manual. AISI S100. Washington, DC: AISI.

AISI (American Iron and Steel Institute). 2012. Specifications for the coldformed steel structural members, cold-formed steel design manual. AISI S100. Washington, DC: AISI.

AISI (American Iron and Steel Institute). 2016. Specifications for the coldformed steel structural members, cold-formed steel design manual. AISI S100. Washington, DC: AISI.

AS/NZS (Australian/New Zealand Standard). 2001. Cold-formed steel structures. AS/NZS 4673. Sydney, Australia: AS/NZS.

AS/NZS (Australian/New Zealand Standard). 2018. Cold-formed steel structures. AS/NZS 4600. Sydney, Australia: AS/NZS.

ASCE (American Society of Civil Engineers). 2002. Specification for the Design of Cold-Formed Stainless Steel Structural Members. SEI/ASCE 8-02. New York: ASCE.

BS EN (British Standards Institution). 2001. Tensile Testing of Metallic Materials Method of Test at Ambient Temperature. 10002-1. London, UK.

CEN (European Committee for Standardization). 2007. Eurocode 9: Design of aluminum structures—Part 1-4: Cold-formed structural sheeting. EN 1999-1-1. Brussels, Belgium: CEN.

Chen, B.S., K. Roy, A. Uzzaman, G.M. Raftery, D. Nash, G.C. Clifton, P. Pouladi, and J.B.P. Lim. 2019. "Effects of edge-stiffened web openings on the behaviour of cold-formed steel channel sections under compression." Thin-Walled Struct. 144: 106307. https://doi.org/10.1016/j.tws.2019.106307.

Chen, Y., R. Feng, and J. Xu. 2017. "Flexural behaviour of CFRP strengthened concrete-filled aluminium alloy CHS tubes." Constr Build Mater. 142: 295-319. https://doi.org/10.1016/j.conbuildmat.2017.03.040.

Chen, Y., R. Feng, and W. Gong. 2018. “Flexural behaviour of concrete-filled aluminium alloy circular hollow section tubes.” Constr Build Mater. 165: 173-186. https://doi.org/10.1016/j.conbuildmat.2017.12.104.

Chi, Y.H., K. Roy, B.S. Chen, Z.Y. Fang, A. Uzzaman, G.B.G. Ananthi and J.B.P. Lim. 2021. “Effect of web hole spacing on axial capacity of back-to-back cold-formed steel channels with edge-stiffened holes.” Steel Compos. Struct. 40(2): 287-305.

Crisan, A., V. Ungureanu, and D. Dubina. 2014. “Calibration of design formula for buckling strength of built-up back-to-back cold-formed steel members in compression.” Procedings of the ICTWS 2014 7th International Conference on Thin Walled Structures, ICTWS, Busan, Korea, 28th September to 2nd October.

Dabaon, M., E. Ellobody, and K. Ramzy. 2015a. “Experimental investigation of built-up cold-formed steel section battened columns.” Thin-Walled Struct. 92: 137-145. https://doi.org/10.1016/j.tws.2015.03.001.

Dabaon, M., E. Ellobody, and K. Ramzy. 2015b. “Nonlinear behaviour of built-up cold-formed steel section battened columns.” J. Constr. Steel Res. 110: 16-28. https://doi.org/10.1016/j.jcsr.2015.03.007.

Dobrić, J., M. Zlatko, B. Dragan, S. Milan, and F. Nenad. 2018a. “Resistance of cold-formed built-up stainless steel columns-Part I: Experiment.” J. Constr. Steel Res. 145: 552-572. https://doi.org/10.1016/j.jcsr.2018.02.026.

Dobrić, J., P. Marko, M. Zlatko, B. Dragan, and S. Milan. 2018b. “Resistance of cold-formed built-up stainless steel columns - Part II: Numerical simulation.” J. Constr. Steel Res. 145: 247-260. https://doi.org/10.1016/j.jcsr.2017.10.032.

Ellobody, E. and B. Young. 2005. “Behaviour of cold-formed steel plain angle columns.” J. Struct. Eng. 131 (3): 469-478. https://doi.org/10.1061/(ASCE)0733-9445(2005)131:3(457).

Faella, C., F.M. Mazzolani, V. Piluso, and G. Rizzano. 2000. “Local buckling of aluminum members: testing and classification.” J. Struct. Eng. 126 (3): 353-360. https://doi.org/10.1061/(ASCE)0733-9445(2000)126:3(353).

Fang, Z.Y., K. Roy, J. Mares, C.-W. Sham, B.S. Chen, and J.B.P. Lim. 2021a. “Deep learning-based axial capacity prediction for cold-formed steel channel sections using Deep Belief Network.” Struct. 33: 2792–2802. https://doi.org/10.1016/j.istruc.2021.05.096.

Fang, Z.Y., K. Roy, B.S. Chen, C.-W. Sham, I. Hajirasouliha, and J.B.P. Lim. 2021b. “Deep learning-based procedure for structural design of cold-formed steel channel sections with edge-stiffened and un-stiffened holes under axial compression.” Thin-Walled Structures. 166: 108076. https://doi.org/10.1016/j.tws.2021.108076.

Feng, R. and B. Young. 2015. “Experimental Investigation of Aluminium Alloy Stub Columns with Circular Openings.” J. Struct. Eng. 141(11): 04015031. https://doi.org/10.1061/(ASCE)ST.1943-541X.0001265.

Feng, R., X. Mou, A. Chen, and Y. Ma. 2016. “Tests of aluminium alloy CHS columns with circular openings.” Thin-Walled Struct. 109: 113-131. https://doi.org/10.1016/j.tws.2016.09.019.

Feng, R., W. Sun, C. Shen, and J. Zhu. 2017. “Experimental investigation of aluminum square and rectangular beams with circular perforations.” Eng. Struct. 151: 613-632. https://doi.org/10.1016/j.engstruct.2017.08.053.

Fratamico, D.C., S. Torabian, X. Zhao, K.J.R. Rasmusen, and B.W. Schafer. 2018. “Experiments on the global and collapse of built-up cold-formed steel columns.” J. Constr. Steel Res. 144: 65-80. https://doi.org/10.1016/j.jcsr.2018.01.007.

Huynh, L.A.T., C.H. Pham, and K.J.R. Rasmussen. 2016a. “Mechanical properties of cold-rolled aluminium alloy 5052 channel sections.” Proceedings of 8th International Conference on Steel and Aluminium Structures. Hong Kong, China 670-684.

Huynh, L.A.T., C.H. Pham, and K.J.R. Rasmussen. 2016b. “Stub column tests and finite element modelling of cold-rolled aluminum alloy 5052 channel sections.” in: Proceedings of the Eighth International Conference on Steel and Aluminum Structures. Hong Kong, China 1–14.

Huynh, L.A.T., C.H. Pham, and K.J.R. Rasmussen. 2019. “Mechanical properties and residual stresses in cold-rolled aluminium channel sections.” Eng. Struct. 199: 109562. https://doi.org/10.1016/j.engstruct.2019.109562.

Huynh, L.A.T., C.H. Pham, and K.J.R. Rasmussen. 2020. “Experimental investigation of cold-rolled aluminium alloy 5052 columns subjected to distortional buckling.” Lecture Notes in Civil Engineering. 54: 287-292. https://doi.org/10.1007/978-981-15-0802-8_43.

International Aluminium Institute, The International Aluminium Institute; 2011. http://www.World-Aluminium.Org/Statistics/.

Kechidi, S., D.C. Fratamico, N. Bourahla, J.M. Castro, and B.W. Schafer. 2017. “Numerical study of screw fasteners in built-up CFS chord studs.” Ce/papers. 1 (2-3): 1543-1552. https://doi.org/10.1002/cepa.197.

Kechidi, S., D.C. Fratamico, B.W. Schafer, and C.J. Miguel. 2020. “Simulation of screw connected built-up cold formed steel back-to-back lipped channels under axial compression.” Eng. Struct. 206: 110109. https://doi.org/10.1016/j.engstruct.2019.110109.

Kesawan, S., M.Mahendran, Y. Dias, and W.B. Zhao. 2017. “Compression tests of built-up cold-formed steel hollow flange sections.” Thin-Walled Struct. 116: 180-193. https://doi.org/10.1016/j.tws.2017.03.004.

Mazzolani, F.M., V. Piluso, and G. Rizzano. 2011. “Local buckling of aluminum alloy angles under uniform compression.” J. Struct. Eng. 137(2): 173-184. https://doi.org/10.1061/(ASCE)ST.1943-541X.0000289.

Miller, W.S., L.Z. Zhuang, J. Bottema, A.J. Wittebrood, D.S. Peter, A. Haszler, and A. Vieregge. 2000. “Recent development in aluminium alloys for the automotive industry.” Mater. Sci. Eng. 280 (1): 37–49. https://doi.org/10.1016/s0921-5093(99)00653-x.

Rondal, J. and M. Niazi. 1990. “Stability of built-up beams and columns with thin -walled members.” J. Constr. Steel Res. 16: 329-335. https://doi.org/10.1016/0143-974X(90)90034-E.

Roy, K., T.C.H. Ting, H.H. Lau, and J.B.P. Lim. 2018a. “Nonlinear behavior of back-to-back gapped built-up cold-formed steel channel sections under compression.” J. Constr. Steel Res. 147: 257-276. https://doi.org/10.1016/j.jcsr.2018.04.007.

Roy, K., T.C.H. Ting, H.H. Lau, and J.B.P. Lim. 2018b. “Experimental investigation into the behaviour of back-to-back gapped built-up cold-formed steel channel sections under compression.” in: Proceedings of the ‘Wei-Wen Yu International Specialty Conference on Cold-Formed Steel Structures. (Nov): 7-8. St. Louis, Missouri, USA.

Roy, K., T.C.H. Ting, H.H. Lau, and J.B.P. Lim. 2018c. “Effect of thickness on the behaviour of axially loaded back-to-back cold-formed steel built-up channel sections-Experimental and numerical investigation.” Struct. 16: 327-346. https://doi.org/10.1016/j.istruc.2018.09.009.

Roy, K., T.C.H. Ting, H.H. Lau, and J.B.P. Lim. 2018d. “Effect of screw spacing into the behaviour of back-to-back cold-formed duplex stainless steel built-up channel sections under compression.” International Conference on Engineering Research and Practice for Steel Construction 2018 (ICSC2018). Sep: 5-7. Hong Kong, China.

Roy, K., H.H. Lau, B.S. Chen, T.C.H. Ting, and J.B.P. Lim. 2019a. “Effect of screw spacing on axial strength of cold-formed steel built-up box sections-numerical investigation and parametric study.” The 2019 World Congress on Advances in Structural Engineering and Mechanics. Sep: 17-21 Jeju, South Korea.

Roy, K., H.H. Lau, and J.B.P. Lim. 2019b. “Finite element modelling of back-to-back built-up cold-formed stainless-steel lipped channels under axial compression.” Steel Compos. Struct. 33: 37-66. http://doi.org/10.12989/scs.2019.33.1.037.

Roy, K. and J.B.P. Lim. 2019c. "Numerical investigation into the buckling behaviour of face-to-face built-up cold-formed stainless steel channel sections under axial compression." Struct. 20: 42-73. https://doi.org/10.1016/j.istruc.2019.02.019.

Roy, K., H.H. Lau, and J.B.P. Lim. 2019d. "Numerical investigations on the axial capacity of back-to-back gapped built-up cold-formed stainless steel channels." Adv. Struct. Eng. 22 (10):2289-2310. https://doi.org/10.1177/1369433219837390.

Roy, K., H. H. Lau, T. C. H. Ting, R. Masood, A. Kumar, and J. B. P. Lim. 2019e. "Experiments and finite element modelling of screw pattern of self-drilling screw connections for high strength cold-formed steel." Thin-Walled Struct. 145 106393. https://doi:10.1016/j.tws.2019.106393.

Roy, K., H. H. Lau, T. C. H. Ting, B. Chen, and J. B. P. Lim. 2020. "Flexural capacity of gapped built-up cold-formed steel channel sections including web stiffeners." J. Constr. Steel Res. 172 106154. https://doi:10.1016/j.jcsr.2020.106154.

Roy, K., B.S. Chen, Z.Y. Fang, A. Uzzaman, X. Chen, and J.B.P. Lim. 2021. "Local and distortional buckling behaviour of back-to-back built-up aluminium alloy channel section columns." Thin-Walled Struct. 163 (1). https://doi.org/10.1016/j.tws.2021.107713.

Su, M.N., B. Young, and L. Gardner. 2013. "Continuous strength method for aluminium alloy structures." Adv. Mat. Res. 742: 70-75. https://doi.org/10.4028/www.scientific.net/AMR.742.70.

Su, M.N., B. Young, and L. Gardner. 2014. "Testing and design of aluminum alloy cross sections in compression." J. Struct. Eng. 140 (9): 04014047. https://doi.org/10.1061/(ASCE)ST.1943-541X.0000972.

Su, M.N., B. Young, and L. Gardner. 2016. "Assessment of Eurocode 9 slenderness limits for elements in compression." Tubular Structures-Proceedings of the 15th International Symposium on Tubular Structures. May 569-574 Rio de Janeiro, Brazil.

Ting, T.C.H., K. Roy, H.H. Lau, and J.B.P. Lim. 2018. “Effect of screw spacing on behaviour of axially loaded back-to-back cold-formed steel built-up channel sections.” Adv. Struct. Eng. 21: 474-487. https://doi.org/10.1177/1369433217719986.

Uzzaman, A., J. B. P. Lim, D. Nash, and K. Roy. 2020a. “Cold-formed steel channel sections under end-two-flange loading condition: Design for edge-stiffened holes, unstiffened holes and plain webs.” Thin-Walled Struct. 147, 106532. https://doi.org/10.1016/j.tws.2019.106532.

Uzzaman, A., J. B. P. Lim, D. Nash, and K. Roy. 2020b. “Web crippling behaviour of cold-formed steel channel sections with edge-stiffened and unstiffened circular holes under interior-two-flange loading condition.” Thin-Walled Struct. 154 106813. https://doi:10.1016/j.tws.2020.106813.

Ye, J., I. Hajirasouliha, J.Becque. 2018a. “Experimental investigation of local-flexural interactive buckling of cold-formed steel channel columns.” Thin-Walled Struct. 125: 245-258. https://doi.org/10.1016/j.tws.2018.01.020.

Ye, J., S.M. Mojtabaei, I. Hajirasouliha. 2018b. “Local-flexural interactive buckling of standard and optimised cold-formed steel columns.” J. Constr. Steel Res. 144: 106-118. https://doi.org/10.1016/j.jcsr.2018.01.012.

Young, B. and W. Hartono. 2002. “Compression tests of stainless steel tubular members.” J. Struct. Eng. 128(6): 754-761. https://doi.org/10.1061/(ASCE)0733-9445(2002)128:6(754).

Young, B. and E. Ellobody. 2005. “Buckling analysis of cold-formed steel lipped angle columns.” J. Struct. Eng. 131(10): 1570-1579. https://doi.org/10.1061/(ASCE)0733-9445(2005)131:10(1570).

Young, B. and E. Ellobody. 2007. “Design of cold-formed steel unequal angle compression members.” Thin-Walled Struct. 45 (3): 330-338. https://doi.org/10.1016/j.tws.2007.02.015.

Yuan, H.X., Y.Q. Wang, Y.J. Shi, and L. Gardner. 2014. “Stub column tests on stainless steel built-up sections.” Thin-Walled Struct. 83: 103-114. https://doi.org/10.1016/j.tws.2014.01.007.

Notations

a	Screw spacing from the AISI 2016 & AS/NZS 2018;
A'	Total length of the web;
A_{eff}	Effective area of the section;
A_g	Gross cross-sectional area;
A_s	Area of the edge stiffener from the CEN 2007;
b	Total width of the plate from the CEN 2007;
b_e	Effective width of the plate from the CEN 2007;
B'	Total length of the flange;
C_1'	Total width of the shorter lip;
C_2'	Total width of the longer lip;
CFS	Cold-formed steel;
COV	Coefficient of variation;
E	Young's modulus of elasticity;
f_c	Stress from the ADM 2020;
f_{oc}	Least of the elastic flexural, torsional, and flexural torsional buckling stress;
f_{cy}	Compressive yield strength from the ADM 2020;
f_e	Least of the elastic flexural, torsional, and flexural torsional buckling stress;
f_0	Characteristic value of 0.2% tensile proof stress from CEN 2007;
f_y	Yield stress from;
F_n	Nominal buckling stress as per the AISI 2016 & AS/NZS 2018;
F_y	Yield stress of the cold-formed steel;
FEA	Finite element analysis;
k_2	Postbuckling constant from the ADM 2020;
$(KL/r)_{ms}$	Modified slenderness;
$(KL/r)_o$	Overall Slenderness from the AISI 2016 & AS/NZS 2018;
L	Total length of the back-to-back built-up aluminium alloy channel sections;
LVDT	Linear variable displacement transducers;
n	Screw number;
P_{ADM}	Axial strength from the ADM 2020;
P'_{ADM}	Axial strength from the improved ADM 2020 considering modified slenderness
$P_{AISI\&AS/NZS}$	ratio;
P_{EXP}	Axial strength by AISI 2016 & AS/NZS 2018;
P_{FEA}	Axial strength from experiments;
P_{EN}	Axial strength from the finite element analysis;
P'_{EN}	Axial strength from the CEN 2007;
P_{cd}	Axial strength from the improved CEN 2007 considering modified slenderness
$P_{n1\&2\&3}$	ratio;
P_y	Elastic distortional compression member buckling load;
r	Strength of the buckling from the ADM 2020;
r_i	Nominal yield capacity of the member in compression;
S	Radius of gyration;
T	Minimum radius of gyration from the AISI 2016 & AS/NZS 2018;
κ	Longitudinal spacing of screw;
γ_{M1}	Nominal thickness of the channel section;
λ_c	Factor for the allowed weakening effects from the CEN 2007;
λ_{eq}	Partial factor from the CEN 2007;
	Non-dimensional slenderness ratio as per the AISI 2016 & AS/NZS 2018;
	Equivalent slenderness ratio from the ADM 2020;

Tables:

Table 1. Axial strength of back-to-back built-up aluminium alloy channel sections

(a) For BU150

Specimen	Web	Flange	Length	Thickness	Spacing	Lip	Modified Slenderness	Experimental results	FEA results		Failure mode
	A'	B'	L	t	S	C'	(KL/r)m	P_{EXP}	P_{FEA}	P_{EXP}/P_{FEA}	
	(mm)	(mm)	(mm)	(mm)	(mm)	-		(kN)	(kN)		
Intermediate											
BU150-S225-L1000	149.93	67.05	998.93	1.57	225.00	25.14	12.30	86.42	84.40	1.01	DB+LB
BU150-S450-L1000	149.65	67.11	998.98	1.57	450.00	25.09	20.05	86.50	83.48	1.04	DB+LB
BU150-S900-L1000	149.76	66.88	998.90	1.57	900.00	24.94	37.62	86.46	84.22	1.03	DB+LB
Mean										1.03	
COV										0.02	
Slender											
BU150-S350-L1500	149.59	66.92	1499.90	1.59	350.00	25.29	18.86	85.61	85.33	1.00	DB+LB
BU150-S700-L1500	149.97	67.00	1499.80	1.58	700.00	24.82	31.08	84.80	84.16	1.01	DB+LB
BU150-S1400-L1500	149.38	66.94	1499.63	1.57	1400.00	24.97	58.36	83.03	83.62	0.99	DB+LB
Mean										1.00	
COV										0.01	

(b) For BU240

Specimen	Web	Flange	Length	Thickness	Spacing	Lip	Modified Slenderness	Experimental results	FEA results		Failure mode
	A'	B'	L	t	S	C'	(KL/r)m	P_{EXP}	P_{FEA}	P_{EXP}/P_{FEA}	
	(mm)	(mm)	(mm)	(mm)	(mm)	-		(kN)	(kN)		
Intermediate											
BU240-S225-L1000	241.35	46.84	1000.08	1.95	225.00	19.90	15.16	105.18	97.21	1.08	DB+GB
BU240-S450-L1000	241.43	46.74	1000.13	1.95	450.00	19.97	28.78	102.43	96.24	1.06	DB+GB
BU240-S900-L1000	241.13	46.59	1000.15	1.95	900.00	20.07	56.85	93.06	95.25	0.98	DB+GB
Mean										1.04	
COV										0.06	
Slender											
BU240-S350-L1500	241.25	46.66	1500.18	1.95	350.00	20.09	23.50	92.08	91.59	1.01	DB+GB
BU240-S700-L1500	241.08	46.82	1500.13	1.94	700.00	20.17	44.54	89.65	88.86	1.01	DB+GB
BU240-S1400-L1500	241.20	46.63	1500.00	1.95	1400.00	20.19	88.23	84.48	86.39	0.98	DB+GB
Mean										1.00	
COV										0.02	

Note: LB=Local buckling; DB=Distortional buckling; GB=Global buckling.

Table 2. Coupon tests sample dimensions

Gauge length (*G*) (mm)	Width (*W*) (mm)	Thickness (*t*) (mm)	Radius of fillet(*R*) (mm)	Overall length (*L*) (mm)	Reduced parallel length (*A*) (mm)	Grip Length (*B*) (mm)	Grip width (*C*) (mm)
50 ± 0.1	12.5 ± 0.2	1.56 ± 0.05	12.6	200	57	50	20

Table 3. Material properties obtained from tensile coupon tests

Coupon ID	initial elastic modulus, *E* (GPa)	Thickness, t (mm)	Ultimate stress f_u (MPa)	Yield stress f_y (MPa)
BU150-1	67551	1.56	122.70	107.90
BU150-2	65101	1.56	123.10	108.90
Mean	66326	1.56	122.80	108.40
BU240-1	65388	1.98	206.40	150.60
BU240-2	65896	1.97	204.80	150.40
Mean	65642	1.98	205.60	150.50

Table 4. Maximum amplitude of local, distortional and overall imperfections

Specimen	Local	Distortional	Global
	(mm)	(mm)	(mm)
BU150-S225-L1000	0.25	1.16	0.86
BU150-S450-L1000	0.46	1.11	0.89
BU150-S900-L1000	0.27	1.14	0.62
BU150-S350-L1500	0.57	1.28	0.58
BU150-S700-L1500	0.32	1.18	0.58
BU150-S1400-L1500	0.95	0.93	0.79
BU240-S225-L1000	0.41	0.87	0.98
BU240-S450-L1000	0.67	0.79	0.64
BU240-S900-L1000	0.62	0.71	0.92
BU240-S350-L1500	0.36	0.69	0.43
BU240-S700-L1500	0.51	1.31	0.93
BU240-S1400-L1500	0.23	0.98	0.87

Table 5. Axial strength predicted from parametric study based on FEA for column modified slenderness, screw number (screw spacing) and section thickness

(a) For BU150

Specimen	Web	Flange	Lip	Length	Thickness	Modified Slenderness			Spacing(s) For			P_{FEA} for		
	A'	B'	C'	L	t	$(KL/r)_m$			3 screws	5 screws	9 screws	3 screws	5 screws	9 screws
	mm	mm	mm	mm	mm	3 screws	5 screws	9 screws	mm	mm	mm	kN	kN	kN
BU150-L1000	150	65	25	1000	1.6	20.68	12.57	9.51	450	225	112.5	84.56	89.64	89.79
					1.8							99.61	100.09	100.6
					2							115.24	114.64	115.83
					2.2							137.20	139.93	140.92
					2.4							154.27	156.70	157.15
					2.6							178.54	179.06	179.11
BU150-L1200	150	65	25	1200	1.6	25.20	15.24	11.47	550	275	137.5	83.69	84.34	84.54
					1.8							98.73	98.48	99.55
					2							114.31	114.21	114.5
					2.2							135.50	137.15	137.89
					2.4							153.33	153.98	154.01
					2.6							176.75	176.84	176.95
BU150-L1500	150	65	25	1500	1.6	26.27	16.95	13.66	700	350	175.0	82.56	84.02	84.28
					1.8							97.81	99.41	99.71
					2							113.96	113.97	114.02
					2.2							134.80	136.13	136.61
					2.4							151.67	151.05	152.45
					2.6							175.54	174.68	174.75
BU150-L1800	150	65	25	1800	1.6	33.02	20.93	16.58	850	425	212.5	83.41	83.46	83.52
					1.8							98.40	98.51	98.88
					2							113.69	113.79	113.98
					2.2							131.86	134.51	134.71
					2.4							148.17	149.45	149.49
					2.6							173.29	174.45	174.48
BU150-L2000	150	65	25	2000	1.6	39.43	24.35	18.77	950	475	237.5	82.16	83.16	83.31
					1.8							97.50	98.28	98.70
					2							112.62	113.71	113.94
					2.2							130.14	131.35	131.77
					2.4							147.18	148.22	148.88
					2.6							171.78	172.32	172.45
BU150-L2500	150	65	25	2500	1.6	45.03	28.74	22.92	1200	600	300.0	81.02	81.43	81.78
					1.8							95.79	96.47	96.49
					2							111.52	112.06	112.33
					2.2							129.23	129.27	129.42
					2.4							146.15	148.01	148.71
					2.6							171.19	171.83	171.91
BU150-L3000	150	65	25	3000	1.6	65.92	39.31	29.08	1450	725	362.5	78.07	78.82	78.88
					1.8							93.69	94.44	94.94
					2							111.03	111.09	110.84
					2.2							127.18	127.91	128.69
					2.4							145.14	146.87	146.99
					2.6							169.75	170.38	170.43

(b) For BU240

Specimen	Web	Flange	Lip	Length	Thickness	Modified Slenderness			Spacing(s) For			P_{FEA} for		
	A'	B'	C'	L	t	$(KL/r)_m$			3 screws	5 screws	9 screws	3 screws	5 screws	9 screws
	mm	mm	mm	mm	mm	3 screws	5 screws	9 screws	mm	mm	mm	kN	kN	kN
BU240-L1000	240	45	20	1000	1.9	28.53	15.07	8.96	450	225	112.5	95.33	95.99	96.57
					2.1							111.22	111.95	112.84
					2.3							125.92	126.07	127.52
					2.5							143.13	143.71	143.91
					2.7							158.83	159.84	160.74
					2.9							184.21	184.78	185.44
BU240-L1200	240	45	20	1200	1.9	34.85	18.37	10.87	550	275	137.5	93.32	93.86	94.47
					2.1							108.55	108.97	109.24
					2.3							123.21	123.89	124.24
					2.5							140.74	141.12	141.68
					2.7							156.6	156.71	157.24
					2.9							182.23	182.87	183.24
BU240-L1500	240	45	20	1500	1.9	35.21	19.05	11.99	700	350	175.0	90.56	91.12	91.98
					2.1							105.41	105.87	106.12
					2.3							120.11	121.12	121.98

					2.5							137.54	138.01	138.26
					2.7							154.23	154.87	155.57
					2.9							180.12	180.45	181.00
BU240-L1800	240	45	20	1800	1.9	44.68	23.98	14.83	850	425	212.5	87.33	87.35	87.57
					2.1							104.11	104.21	105.77
					2.3							117.74	118.54	119.12
					2.5							133.57	134.27	134.86
					2.7							153.11	153.50	154.00
					2.9							177.83	178.12	178.89
BU240-L2000	240	45	20	2000	1.9	54.02	28.70	17.32	950	475	237.5	85.47	85.78	85.95
					2.1							102.64	103.53	104.95
					2.3							115.44	115.91	116.13
					2.5							132.15	132.56	133.02
					2.7							152.04	152.59	152.98
					2.9							175.35	176.07	176.53
BU240-L2500	240	45	20	2500	1.9	60.70	32.68	20.35	1200	600	300.0	83.53	84.60	85.27
					2.1							101.15	101.57	101.98
					2.3							113.77	113.89	114.07
					2.5							130.27	130.35	130.59
					2.7							151.00	151.97	152.68
					2.9							173.47	173.73	174.50

Note: LB=Local buckling; DB=Distortional buckling; GB=Global buckling.

Table 6. Comparisons of axial strength between numerical, experimental, and theoretical investigations

(a) For BU150

Specimen	Experimental results	Comparison					
	P_{EXP} (kN)	P_{EXP}/P_{FEA}	P_{EXP}/P_{ADM}	P_{EXP}/P_{EN}	$P_{EXP}/P_{AISI\&AS/NZS}$	P_{EXP}/P'_{ADM}	P_{EXP}/P'_{EN}
Intermediate							
BU150-S225-L1000	86.42	1.01	0.96	1.20	0.96	0.93	1.16
BU150-S450-L1000	86.50	1.04	0.96	1.20	0.96	0.95	1.17
BU150-S900-L1000	86.46	1.03	1.01	1.20	0.97	1.00	1.19
Mean		1.03	0.98	1.20	0.96	0.96	1.18
COV		0.02	0.02	0.00	0.00	0.03	0.02
Slender							
BU150-S350-L1500	85.61	1.00	1.03	1.27	1.06	0.98	1.19
BU150-S700-L1500	84.80	1.01	1.03	1.27	1.07	1.01	1.22
BU150-S1400-L1500	83.03	0.99	1.11	1.26	1.05	1.11	1.25
Mean		1.00	1.06	1.26	1.06	1.04	1.22
COV		0.01	0.04	0.01	0.01	0.06	0.02

(b) For BU240

Specimen	Experimental results	Comparison					
	P_{EXP} (kN)	P_{EXP}/P_{FEA}	P_{EXP}/P_{ADM}	P_{EXP}/P_{EN}	$P_{EXP}/P_{AISI\&AS/NZS}$	P_{EXP}/P'_{ADM}	P_{EXP}/P'_{EN}
Intermediate							
BU240-S225-L1000	105.18	1.08	1.50	1.03	1.09	1.41	0.98
BU240-S450-L1000	102.43	1.06	1.46	1.00	1.12	1.38	0.98
BU240-S900-L1000	93.06	0.98	1.33	0.91	1.02	1.25	0.98
Mean		1.04	1.43	0.98	1.08	1.34	0.98
COV		0.05	0.07	0.05	0.05	0.07	0.00
Slender							
BU240-S350-L1500	92.08	1.01	1.32	1.08	1.01	1.23	0.99
BU240-S700-L1500	89.65	1.01	1.29	1.06	0.99	1.21	1.02
BU240-S1400-L1500	84.48	0.98	1.21	1.05	0.93	1.13	1.01
Mean		1.00	1.27	1.06	0.98	1.19	1.00
COV		0.02	0.05	0.01	0.04	0.04	0.02

Note: LB=Local buckling; DB=Distortional buckling; GB=Global buckling.

Table 7. Comparison of FE results obtained from parametric study and design strength for varying column modified slenderness, screw number (screw spacing) and section thickness

(a) For BU150

Specimen	Thickness	P_{FEA} for			P_{FEA}/P_{ADM}			P_{FEA}/P_{EN}			$P_{FEA}/P_{AISI\&AS/NZS}$			P_{FEA}/P'_{ADM}			P_{FEA}/P'_{EN}		
	t	3 screws	5 screws	9 screws	3 screws	5 screws	9 screws	3 screws	5 screws	9 screws	3 screws	5 screws	9 screws	3 screws	5 screws	9 screws	3 screws	5 screws	9 screws
	mm	kN	kN	kN															
BU150-L1000	1.6	84.56	89.64	89.79	0.94	1.00	1.00	1.27	1.34	1.35	1.07	1.07	1.08	0.93	0.97	0.97	1.13	1.18	1.17
	1.8	99.61	100.09	100.60	0.99	0.99	1.00	1.23	1.24	1.24	1.02	1.02	1.02	0.98	0.96	0.96	1.09	1.08	1.08
	2	115.24	114.64	115.83	1.03	1.02	1.03	1.20	1.20	1.21	1.01	1.02	1.03	1.02	0.99	1.00	1.07	1.04	1.05
	2.2	137.20	139.93	140.92	1.11	1.13	1.14	1.26	1.28	1.29	1.08	1.09	1.10	1.10	1.10	1.10	1.11	1.12	1.12
	2.4	154.27	156.70	157.15	1.15	1.16	1.17	1.27	1.29	1.29	1.08	1.09	1.09	1.14	1.13	1.13	1.12	1.12	1.12
	2.6	178.54	179.06	179.11	1.22	1.23	1.23	1.33	1.33	1.33	1.13	1.13	1.13	1.21	1.19	1.19	1.17	1.16	1.15
BU150-L1200	1.6	83.69	84.34	84.54	0.97	0.98	0.98	1.30	1.31	1.31	1.01	1.01	1.01	0.96	0.94	0.94	1.15	1.13	1.13
	1.8	98.73	98.48	99.55	1.02	1.01	1.03	1.27	1.26	1.28	1.00	1.00	1.01	1.01	0.98	0.98	1.12	1.09	1.10
	2	114.31	114.21	114.50	1.06	1.06	1.06	1.24	1.24	1.24	1.01	1.01	1.01	1.05	1.02	1.02	1.09	1.07	1.06
	2.2	135.50	137.15	137.89	1.14	1.15	1.16	1.29	1.31	1.32	1.07	1.07	1.08	1.13	1.11	1.11	1.14	1.13	1.13
	2.4	153.33	153.98	154.01	1.18	1.19	1.19	1.31	1.32	1.32	1.07	1.07	1.07	1.17	1.15	1.14	1.15	1.13	1.13
	2.6	176.75	176.84	176.95	1.26	1.26	1.26	1.37	1.37	1.37	1.11	1.11	1.11	1.25	1.22	1.21	1.20	1.18	1.17
BU150-L1500	1.6	82.56	84.02	84.28	1.01	1.03	1.04	1.35	1.38	1.38	1.00	1.01	1.01	0.99	0.98	0.98	1.17	1.17	1.17
	1.8	97.81	99.41	99.71	1.07	1.09	1.09	1.33	1.35	1.36	1.00	1.01	1.02	1.04	1.03	1.03	1.14	1.14	1.14
	2	113.96	113.97	114.02	1.12	1.12	1.12	1.32	1.32	1.32	1.01	1.01	1.01	1.09	1.07	1.06	1.13	1.11	1.10
	2.2	134.80	136.13	136.61	1.20	1.21	1.22	1.37	1.39	1.39	1.06	1.06	1.07	1.17	1.16	1.15	1.17	1.16	1.16
	2.4	151.67	151.05	152.45	1.24	1.23	1.24	1.38	1.38	1.39	1.05	1.05	1.06	1.21	1.18	1.18	1.18	1.16	1.16
	2.6	175.54	174.68	174.75	1.32	1.31	1.31	1.45	1.44	1.44	1.10	1.10	1.10	1.29	1.26	1.25	1.24	1.21	1.20
BU150-L1800	1.6	83.41	83.46	83.52	1.09	1.09	1.09	1.46	1.46	1.46	0.99	1.00	1.00	1.06	1.03	1.02	1.24	1.21	1.20
	1.8	98.40	98.51	98.88	1.14	1.14	1.15	1.43	1.43	1.44	1.00	1.00	1.01	1.11	1.08	1.07	1.21	1.18	1.18
	2	113.69	113.79	113.98	1.18	1.19	1.19	1.41	1.41	1.41	1.01	1.01	1.01	1.15	1.12	1.11	1.19	1.16	1.15
	2.2	131.86	134.51	134.71	1.25	1.27	1.27	1.44	1.47	1.47	1.05	1.05	1.05	1.22	1.20	1.20	1.22	1.21	1.20
	2.4	148.17	149.45	149.49	1.28	1.29	1.29	1.36	1.37	1.37	1.04	1.04	1.04	1.25	1.23	1.22	1.22	1.20	1.19
	2.6	173.29	174.45	174.48	1.38	1.39	1.39	1.44	1.45	1.45	1.09	1.10	1.10	1.35	1.32	1.31	1.31	1.27	1.26
BU150-L2000	1.6	82.16	83.16	83.31	1.12	1.13	1.14	1.50	1.52	1.52	0.98	1.00	1.00	1.09	1.06	1.05	1.27	1.24	1.24
	1.8	97.50	98.28	98.70	1.18	1.19	1.19	1.49	1.50	1.51	0.99	1.00	1.01	1.15	1.11	1.11	1.25	1.22	1.21
	2	112.62	113.71	113.94	1.22	1.23	1.24	1.47	1.48	1.49	1.01	1.01	1.01	1.20	1.16	1.15	1.23	1.20	1.19
	2.2	130.14	131.35	131.77	1.28	1.29	1.30	1.44	1.45	1.45	1.03	1.03	1.03	1.26	1.22	1.21	1.26	1.22	1.21
	2.4	147.18	148.22	148.88	1.32	1.33	1.34	1.35	1.36	1.37	1.03	1.03	1.04	1.30	1.26	1.25	1.23	1.24	1.23
	2.6	171.78	172.32	172.45	1.42	1.43	1.43	1.43	1.43	1.43	1.08	1.08	1.08	1.35	1.35	1.34	1.30	1.30	1.29
BU150-L2500	1.6	81.02	81.43	81.78	1.24	1.24	1.25	1.69	1.70	1.70	0.97	0.98	0.98	1.18	1.14	1.13	1.36	1.32	1.31
	1.8	95.79	96.47	96.49	1.29	1.30	1.30	1.68	1.69	1.70	1.03	0.98	0.98	1.24	1.20	1.18	1.35	1.30	1.28
	2	111.52	112.06	112.33	1.35	1.36	1.36	1.69	1.70	1.70	1.00	0.99	1.01	1.30	1.25	1.24	1.34	1.29	1.28
	2.2	129.23	129.27	129.42	1.41	1.41	1.41	1.43	1.43	1.43	1.00	1.01	1.01	1.37	1.31	1.30	1.30	1.30	1.30
	2.4	146.15	148.01	148.71	1.46	1.47	1.48	1.34	1.36	1.37	1.03	1.03	1.04	1.42	1.38	1.37	1.22	1.24	1.24

	2.6	171.19	171.83	171.91	1.56	1.57	1.57	1.42	1.43	1.43	1.08	1.08	1.08	1.47	1.48	1.46	1.29	1.30	1.30
BU150-L3000	1.6	78.07	78.82	78.88	1.54	1.56	1.56	1.89	1.91	1.91	1.02	0.94	1.03	1.54	1.23	1.20	1.53	1.41	1.38
	1.8	93.69	94.44	94.94	1.61	1.62	1.63	1.94	1.95	1.96	1.00	1.01	1.02	1.65	1.31	1.29	1.55	1.42	1.39
	2	111.03	111.09	110.84	1.67	1.68	1.67	1.74	1.74	1.74	1.00	1.00	1.00	1.76	1.39	1.35	1.58	1.44	1.40
	2.2	127.18	127.91	128.69	1.70	1.71	1.72	1.40	1.41	1.42	0.99	1.00	1.01	1.83	1.46	1.43	1.28	1.28	1.29
	2.4	145.14	146.87	146.99	1.73	1.75	1.75	1.33	1.35	1.35	1.02	1.02	1.02	1.91	1.53	1.50	1.21	1.23	1.23
	2.6	169.75	170.38	170.43	1.81	1.82	1.82	1.41	1.42	1.42	1.07	1.07	1.07	1.64	1.64	1.60	1.28	1.29	1.29

(b) For BU240

Specimen	Thickness	P_{FEA} for			P_{FEA}/P_{ADM}			P_{FEA}/P_{EN}			$P_{FEA}/P_{AISI\&AS/NZS}$			P_{FEA}/P'_{ADM}			P_{FEA}/P'_{EN}		
	t	3 screws	5 screws	9 screws	3 screws	5 screws	9 screws	3 screws	5 screws	9 screws	3 screws	5 screws	9 screws	3 screws	5 screws	9 screws	3 screws	5 screws	9 screws
	mm	kN	kN	kN															
BU240-L1000	1.9	95.33	95.99	96.57	1.44	1.45	1.45	1.09	1.10	1.11	1.12	1.13	1.14	1.35	1.36	1.37	1.07	1.05	1.05
	2.1	111.22	111.95	112.84	1.46	1.47	1.48	1.09	1.00	1.01	1.12	1.13	1.14	1.37	1.38	1.39	1.09	1.07	1.07
	2.3	125.92	126.07	127.52	1.45	1.45	1.47	0.98	1.12	1.13	1.11	1.11	1.12	1.36	1.36	1.38	0.98	0.99	1.00
	2.5	143.13	143.71	143.91	1.47	1.47	1.47	1.01	0.92	0.92	1.10	1.11	1.11	1.37	1.38	1.38	1.01	1.01	1.01
	2.7	158.83	159.84	160.74	1.45	1.46	1.47	1.01	0.93	0.93	1.09	1.10	1.10	1.36	1.37	1.38	1.01	1.02	1.02
	2.9	184.21	184.78	185.44	1.52	1.52	1.53	1.07	0.98	0.98	1.13	1.14	1.14	1.42	1.42	1.43	1.07	1.08	1.08
BU240-L1200	1.9	93.32	93.86	94.47	1.41	1.41	1.42	1.15	1.15	1.16	1.10	1.10	1.11	1.32	1.33	1.34	1.12	1.09	1.09
	2.1	108.55	108.97	109.24	1.42	1.43	1.43	1.07	0.97	0.98	1.10	1.10	1.10	1.34	1.34	1.34	1.07	1.07	1.07
	2.3	123.21	123.89	124.24	1.42	1.43	1.43	0.96	0.88	0.88	1.08	1.09	1.09	1.33	1.34	1.34	0.96	0.97	0.97
	2.5	140.74	141.12	141.68	1.44	1.44	1.45	0.99	0.90	0.90	1.09	1.09	1.09	1.35	1.35	1.36	0.99	0.99	1.00
	2.7	156.60	156.71	157.24	1.43	1.43	1.44	1.00	0.91	0.91	1.07	1.07	1.08	1.34	1.34	1.35	1.00	1.00	1.00
	2.9	182.23	182.87	183.24	1.50	1.51	1.51	1.06	0.97	0.97	1.12	1.12	1.13	1.40	1.41	1.41	1.06	1.07	1.07
BU240-L1500	1.9	90.56	91.12	91.98	1.36	1.37	1.39	1.26	1.16	1.17	1.07	1.07	1.08	1.28	1.29	1.30	1.19	1.15	1.15
	2.1	105.41	105.87	106.12	1.38	1.39	1.39	1.04	0.95	0.95	1.07	1.07	1.07	1.30	1.30	1.31	1.04	1.04	1.04
	2.3	120.11	121.12	121.98	1.39	1.40	1.41	0.94	0.86	0.87	1.05	1.06	1.07	1.30	1.31	1.32	0.94	0.95	0.95
	2.5	137.54	138.01	138.26	1.41	1.41	1.42	0.97	0.88	0.88	1.06	1.07	1.07	1.32	1.32	1.32	0.97	0.97	0.97
	2.7	154.23	154.87	155.57	1.41	1.42	1.42	0.98	0.90	0.90	1.06	1.06	1.07	1.32	1.33	1.33	0.98	0.99	0.99
	2.9	180.12	180.45	181.00	1.48	1.49	1.49	1.05	0.96	0.96	1.11	1.11	1.11	1.39	1.39	1.39	1.05	1.05	1.05
BU240-L1800	1.9	87.33	87.35	87.57	1.32	1.32	1.32	1.22	1.11	1.11	1.01	1.02	1.02	1.24	1.24	1.24	1.22	1.22	1.22
	2.1	104.11	104.21	105.77	1.37	1.37	1.39	1.02	0.93	0.94	1.05	1.05	1.07	1.28	1.28	1.30	1.02	1.02	1.04
	2.3	117.74	118.54	119.12	1.36	1.37	1.37	0.92	0.84	0.85	1.03	1.04	1.05	1.27	1.28	1.29	0.92	0.93	0.93
	2.5	133.57	134.27	134.86	1.37	1.37	1.38	0.94	0.86	0.86	1.03	1.04	1.04	1.28	1.29	1.29	0.94	0.94	0.95
	2.7	153.11	153.50	154.00	1.40	1.41	1.41	0.98	0.89	0.89	1.05	1.05	1.06	1.31	1.31	1.32	0.98	0.98	0.98
	2.9	177.83	178.12	178.89	1.47	1.47	1.47	1.04	0.94	0.95	1.09	1.09	1.10	1.37	1.37	1.38	1.04	1.04	1.04
BU240-L2000	1.9	85.47	85.78	85.95	1.29	1.29	1.29	1.19	1.09	1.09	1.01	1.01	1.01	1.21	1.22	1.22	1.19	1.20	1.20
	2.1	102.64	103.53	104.95	1.35	1.36	1.38	1.01	0.92	0.94	1.04	1.05	1.06	1.26	1.27	1.29	1.01	1.02	1.03
	2.3	115.44	115.91	116.13	1.33	1.34	1.34	0.90	0.82	0.83	1.01	1.02	1.02	1.25	1.25	1.26	0.90	0.91	0.91
	2.5	132.15	132.56	133.02	1.35	1.36	1.36	0.93	0.85	0.85	1.02	1.02	1.03	1.27	1.27	1.27	0.93	0.93	0.93
	2.7	152.04	152.59	152.98	1.39	1.40	1.40	0.97	0.88	0.89	1.04	1.05	1.05	1.30	1.31	1.31	0.97	0.97	0.97

	2.9	175.35	176.07	176.53	1.45	1.45	1.46	1.02	0.93	0.93	1.08	1.08	1.08	1.35	1.35	1.36	1.02	1.03	1.03
BU240-L2500	1.9	83.53	84.60	85.27	1.26	1.27	1.28	1.16	1.07	1.08	0.99	1.00	1.00	1.18	1.20	1.21	1.16	1.18	1.19
	2.1	101.15	101.57	101.98	1.33	1.33	1.34	0.99	0.91	0.91	1.02	1.03	1.03	1.25	1.25	1.26	0.99	1.00	1.00
	2.3	113.77	113.89	114.07	1.31	1.31	1.32	0.89	0.81	0.81	0.99	1.00	1.00	1.23	1.23	1.23	0.89	0.89	0.89
	2.5	130.27	130.35	130.59	1.33	1.33	1.34	0.92	0.83	0.83	1.01	1.01	1.01	1.25	1.25	1.25	0.92	0.92	0.92
	2.7	151.00	151.97	152.68	1.38	1.39	1.40	0.96	0.88	0.88	1.04	1.04	1.05	1.29	1.30	1.31	0.96	0.97	0.97
	2.9	173.47	173.73	174.50	1.43	1.43	1.44	1.01	0.92	0.92	1.07	1.07	1.07	1.33	1.34	1.34	1.01	1.01	1.02

Figures:

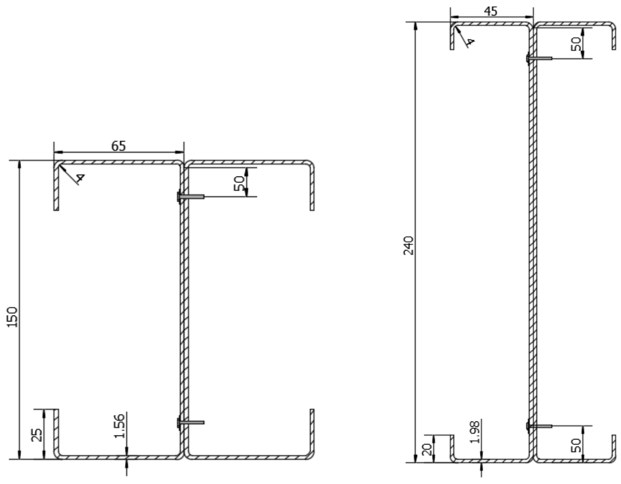

(a) BU150 (t=1.56mm) (b) BU240 (t=1.98mm)

All dimensions are in mm

Fig.1. Nominal cross-sections of the aluminium alloy built-up channel sections considered in this paper

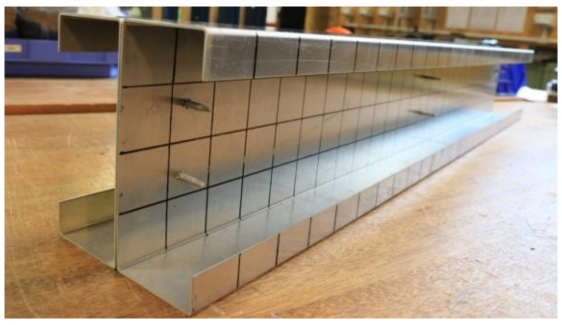

Fig.2. Photograph of the back-to-back built-up aluminium alloy channel sections

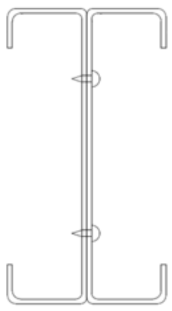

Fig.3. Back-to-back built-up CFS channel columns investigated by Ting et al. (2018)

Fig.4. Back-to-back gapped built-up CFS channel sections investigated by Roy et al. (2018a,b)

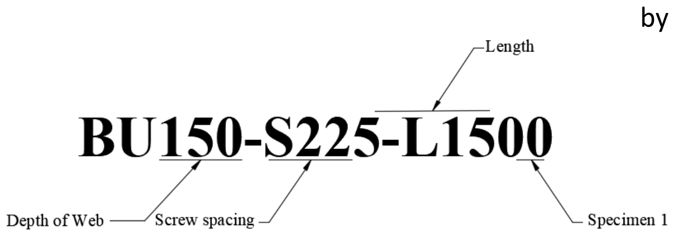

Fig.5. Specimen labelling

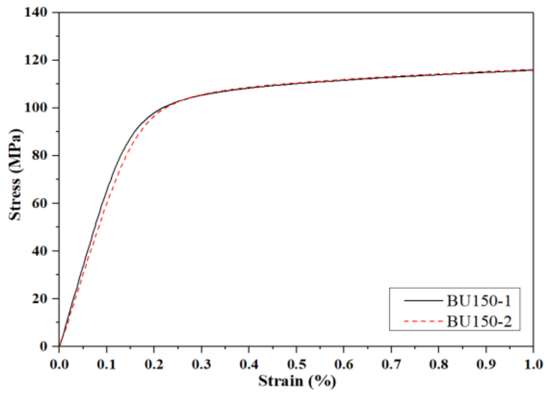

(a) Initial stress–strain curve of BU150

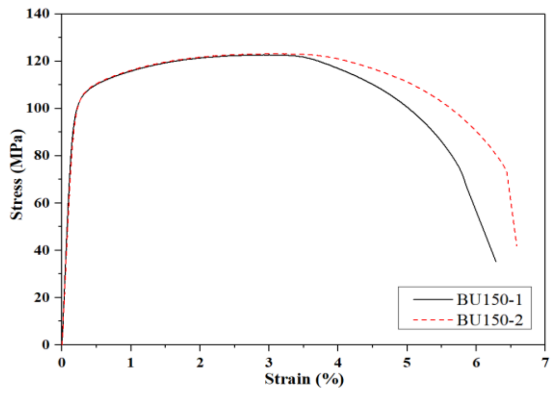

(b) Full stress–strain curve of BU150

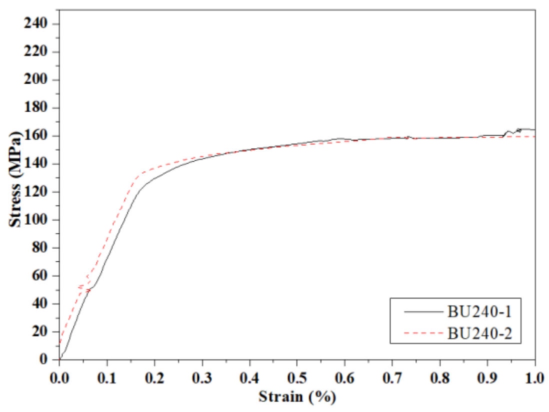

(c) Initial stress–strain curve of BU240

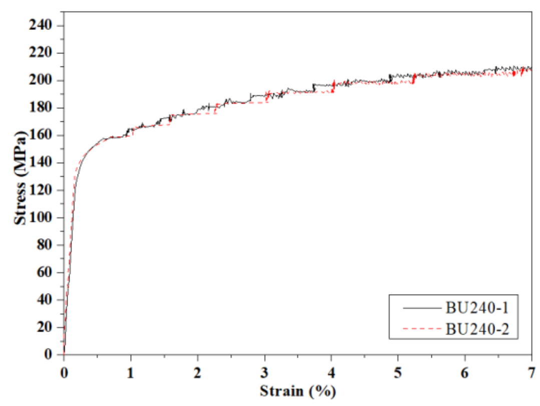

(d) Full stress–strain curve of BU240

Fig.6. Stress-strain curves

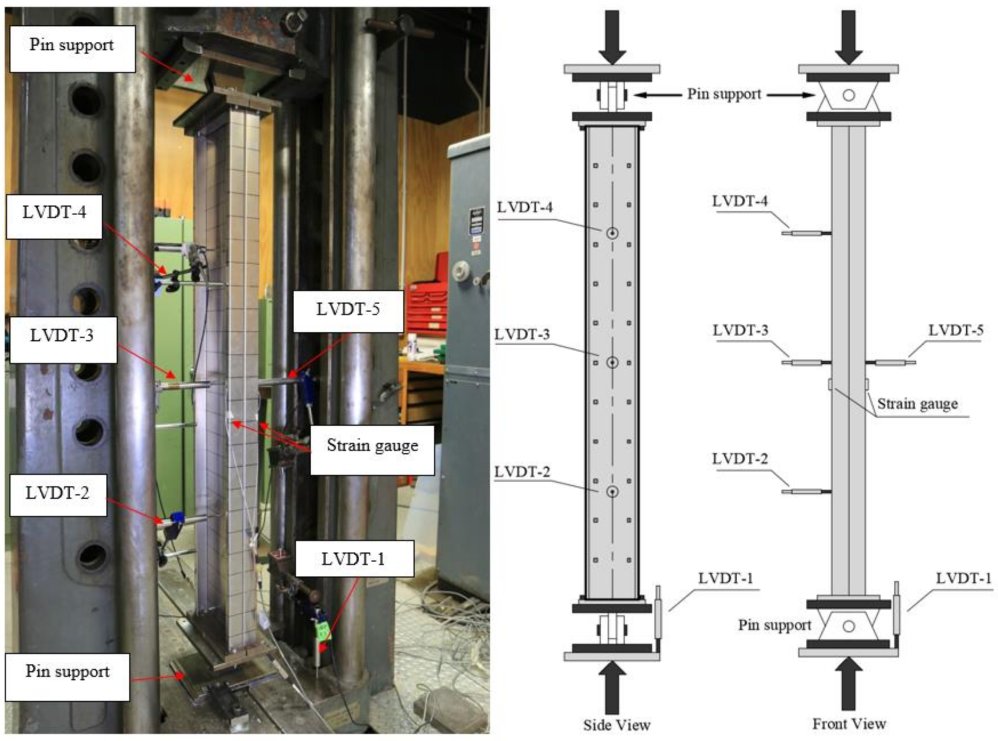

Fig.7. Photograph and schematic drawings of the test set-up

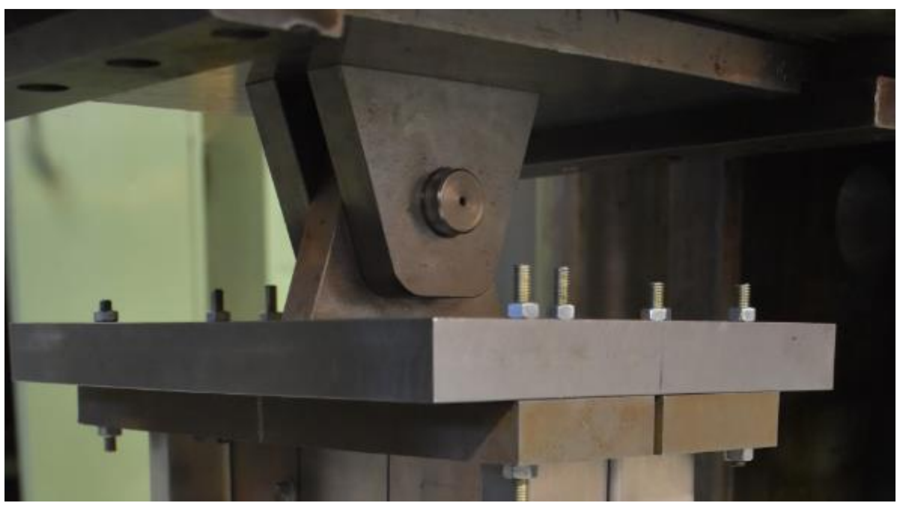

Fig.8. Pin support used in the experiments.

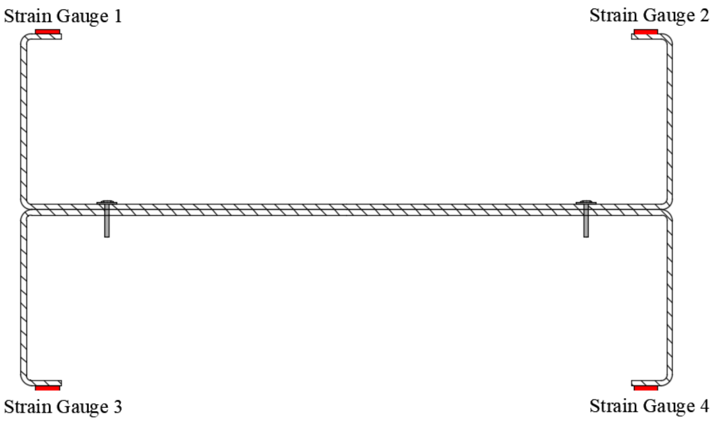

Fig.9. Locations of the strain gauges at mid-height

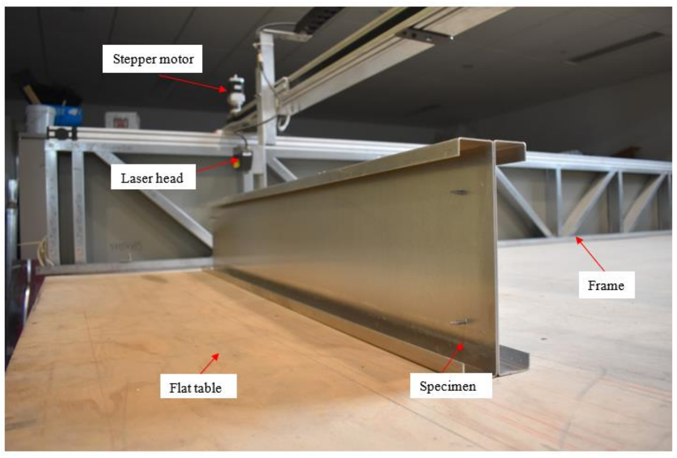

Fig.10. Photograph of imperfection measurements setup

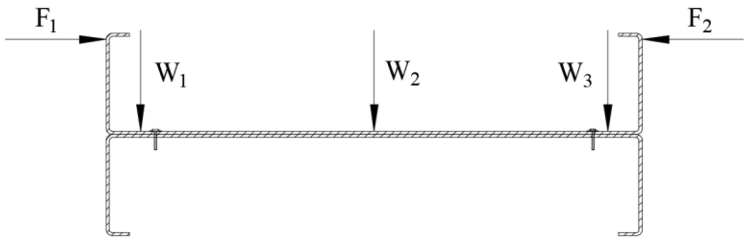

Fig.11. Locations of the geometric imperfection measurements

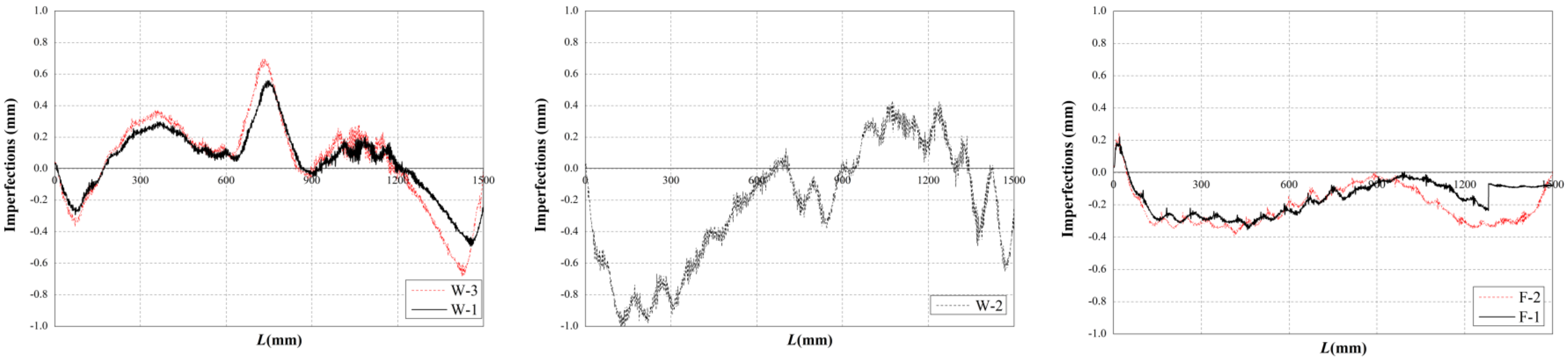

(a) Imperfection of W-1 and W-3

(b) Imperfection of W-2

(c) Imperfection of F-1 and F-2

Fig.12. Typical imperfection profile (BU240-S350-L1500)

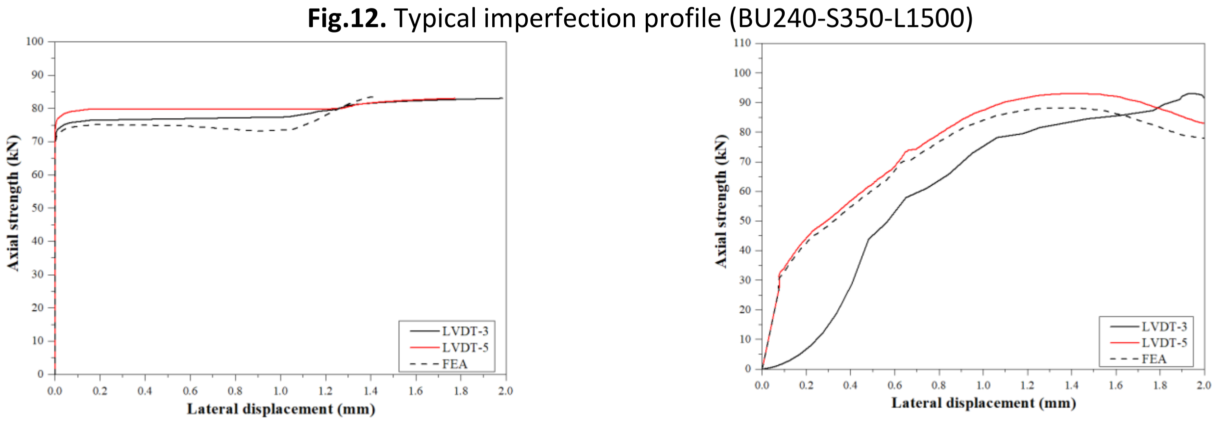

(a) BU150-S1400-L1500

(b) BU240-S900-L1000

Fig.13. Axial load versus lateral deflection relationship at mid-height of specimens

(a) BU150-S900-L1000

(b) BU150-S1400-L1500

(c) BU240-S450-L1000

(d) BU240-S700-L1500

Fig.14. Test pictures of the 1000- and 1500mm-length BU150 and BU240

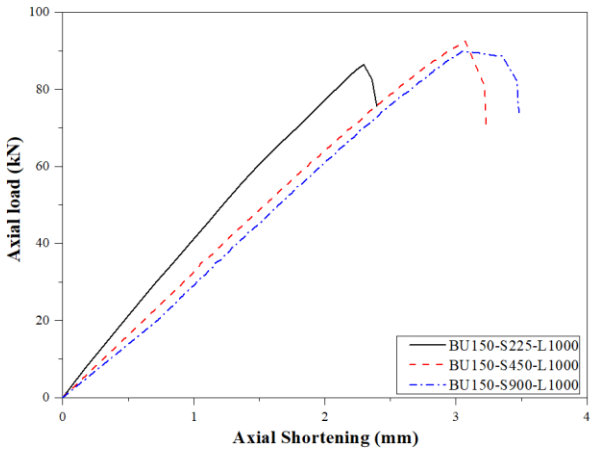

(i) BU150-L1000

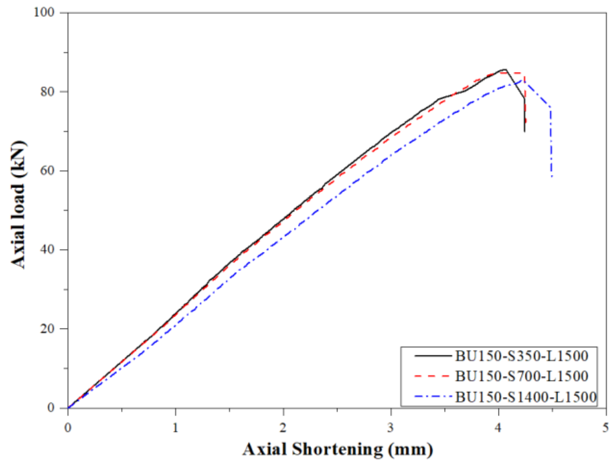

(ii) BU150-L1500

(a) Load-displacement curves for columns of BU150

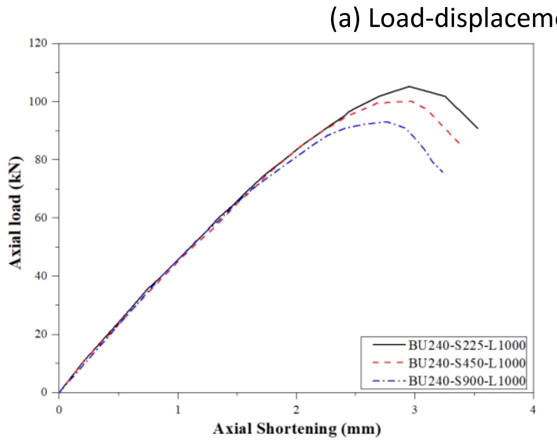

(i) BU240-L1000

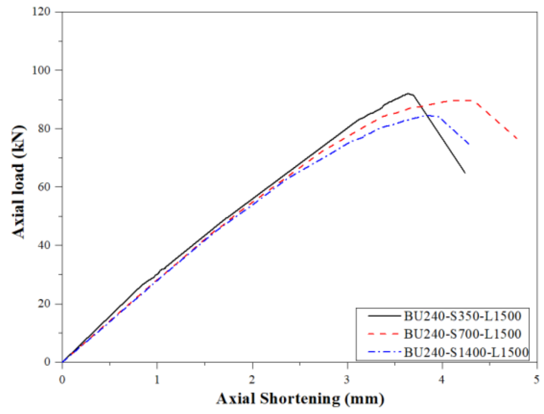

(ii) BU240-L1500

(b) Load-displacement curves for columns of BU240

Fig.15. Axial load versus axial shortening curves of specimens with different column lengths

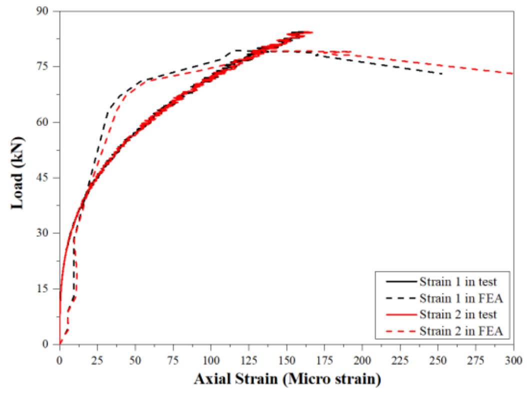

Fig.16. Load versus axial-strain relationship for BU240-S1400-L1500

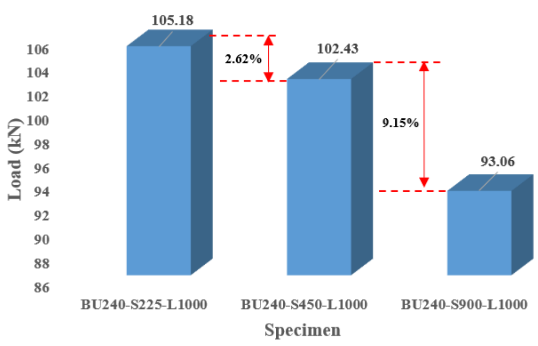

(a) BU240-L1000

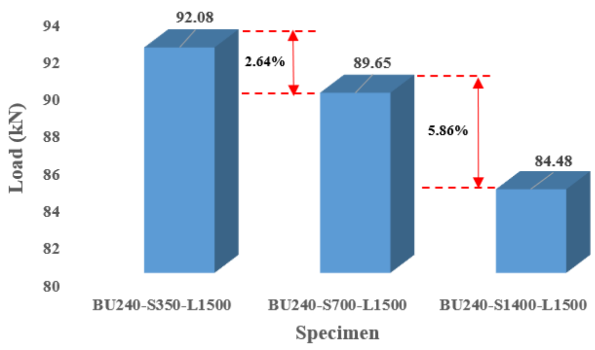

(b) BU240-L1500

Fig.17. Effect of screw spacing on axial strength of back-to-back built-up aluminium alloy channel sections


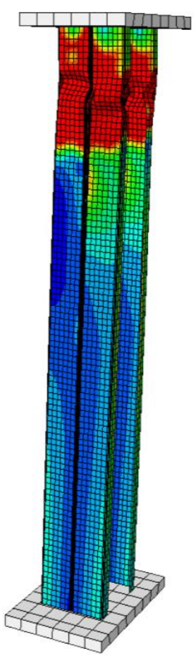

(i) Test (ii) FEA

(a) BU150-S225-L1000


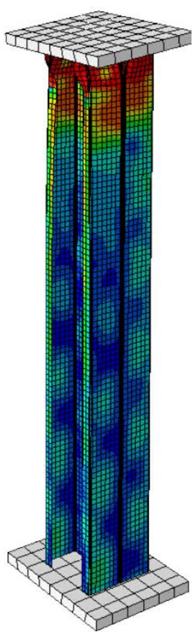

(i) Test (ii) FEA

(b) BU150-S450-L1000


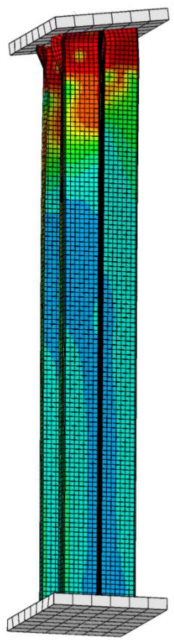

(i) Test (ii) FEA

(c) BU150-S900-L1000

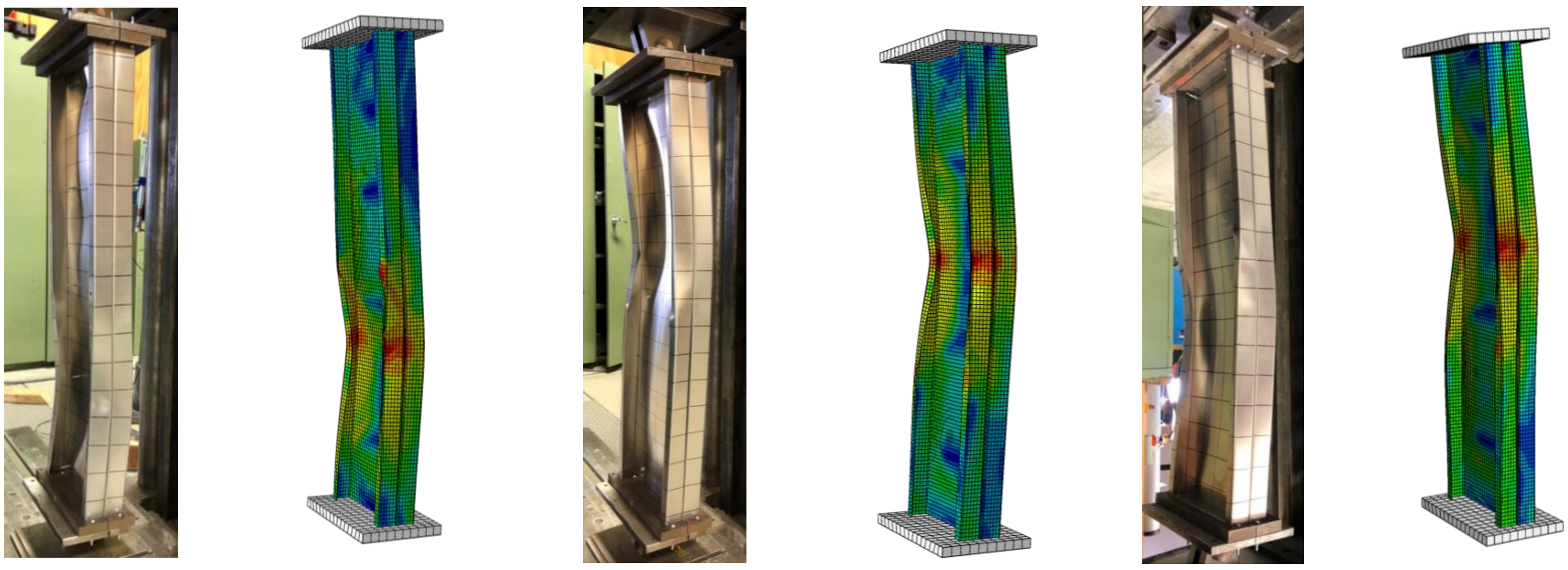

(i) Test (ii) FEA
(d) BU240-S225-L1000

(i) Test (ii) FEA
(e) BU240-S450-L1000

(i) Test (ii) FEA
(f) BU240-S900-L1000

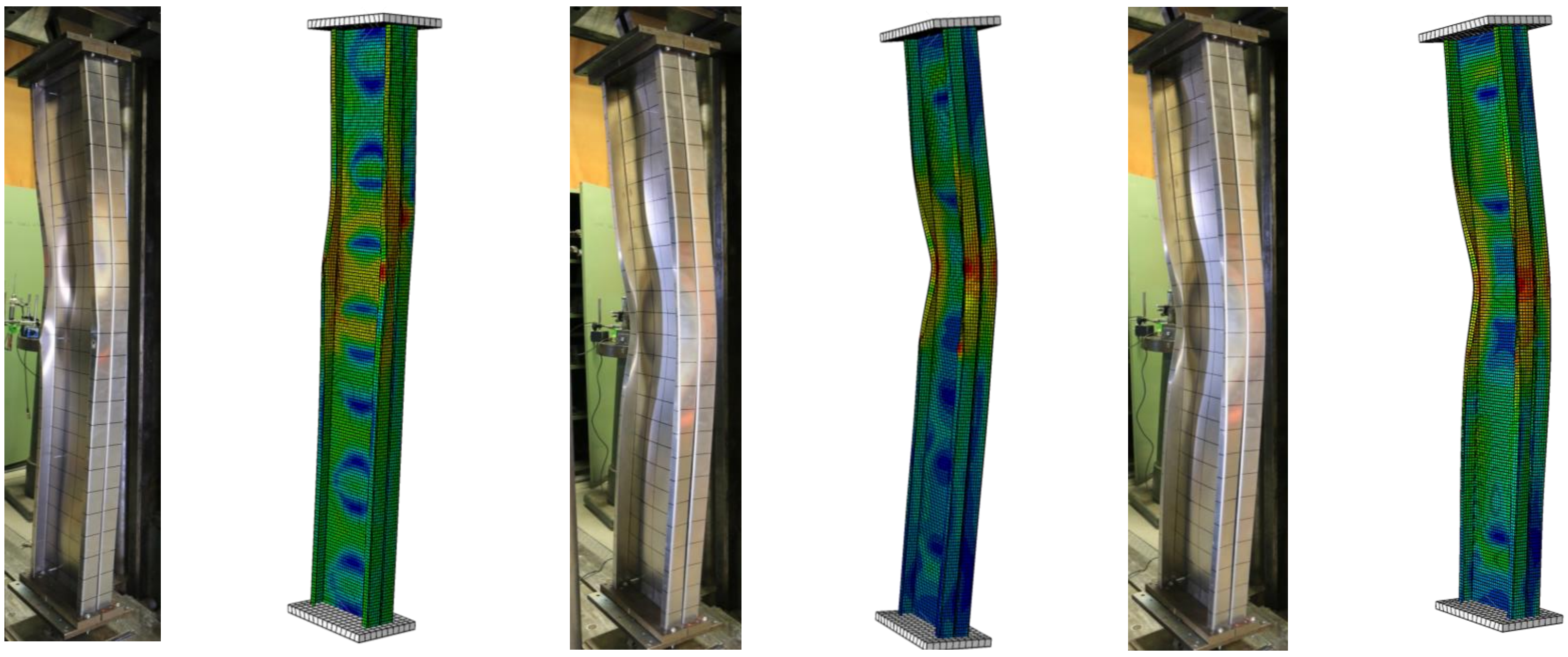

(i) Test (ii) FEA
(g) BU240-S350-L1500

(i) Test (ii) FEA
(h) BU240-S700-L1500

(i) Test (ii) FEA
(i) BU240-S1400-L1500

Fig.18. Deformed shapes at failure from experiments and FEA

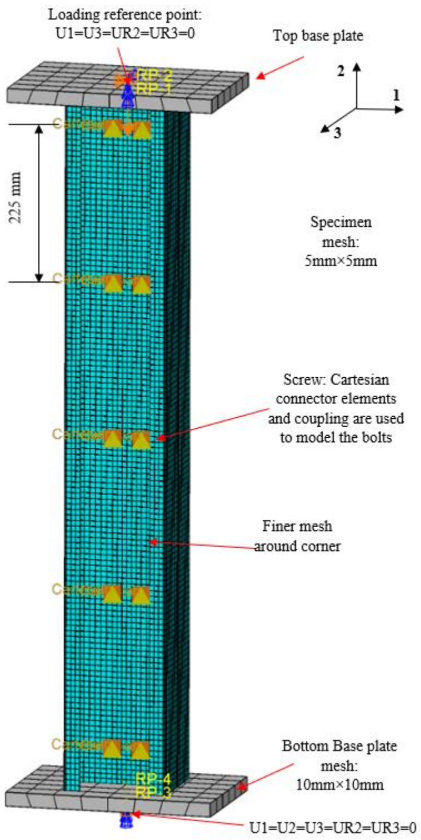

(a) Mesh type and boundary condition applied in the FE model for BU150-S225-L1000

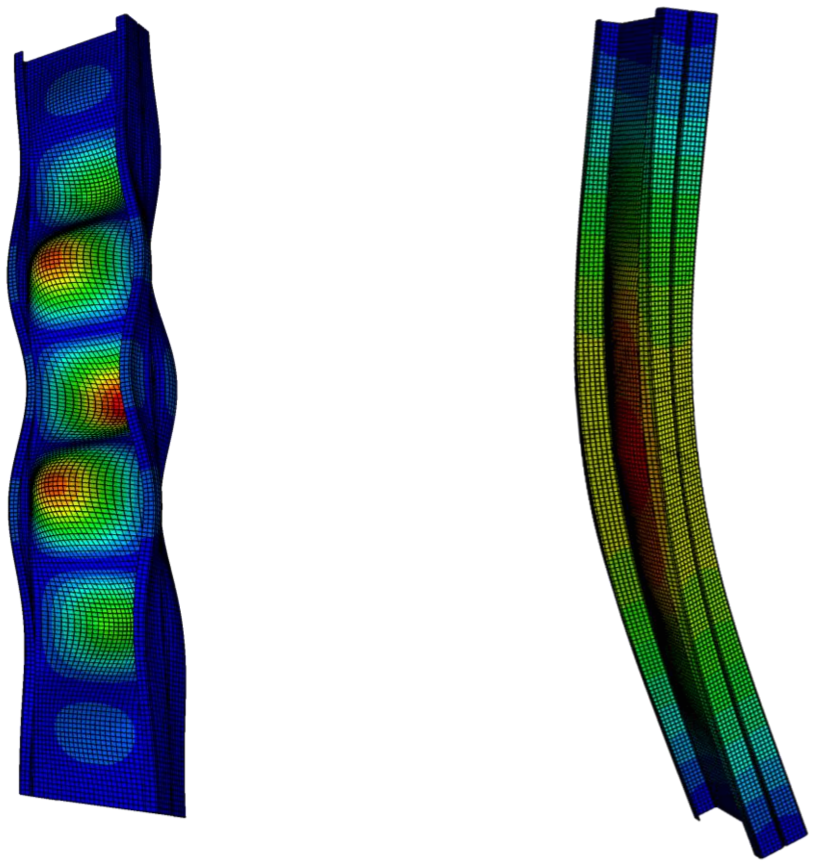

(i) Local buckling (ii) Global buckling
(b) Buckling type

Fig.19. Details of the FE model

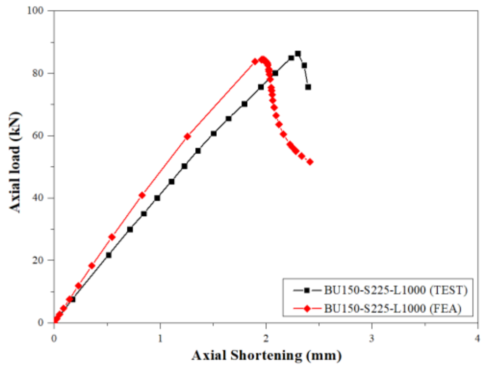

(a) BU150-S225-L1000

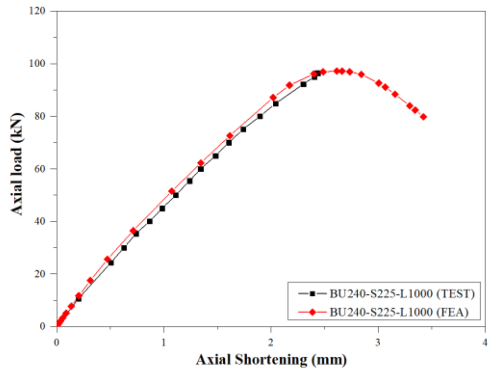

(b) BU240-S225-L1000

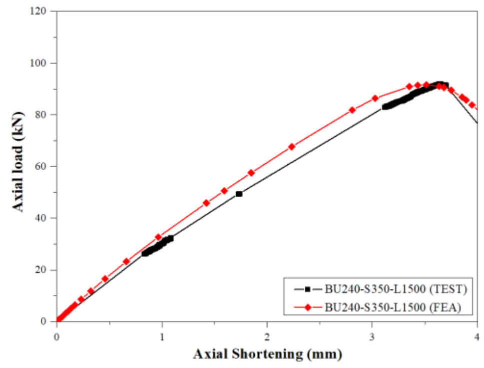

(c) BU240-S350-L1500

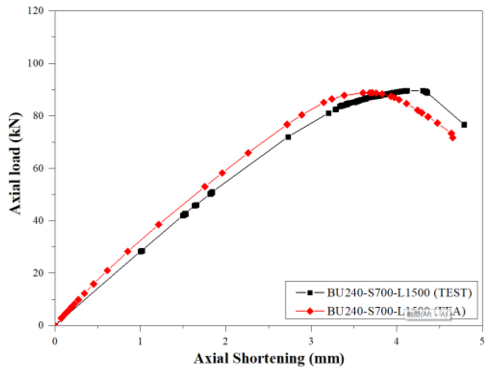

(d) BU240-S700-L1500

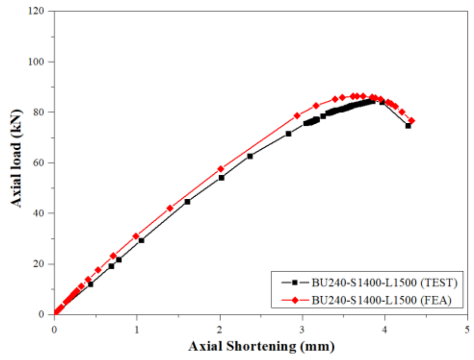

(e) BU240-S1400-L1500

Fig.20. Load versus axial-shortening relationship for columns

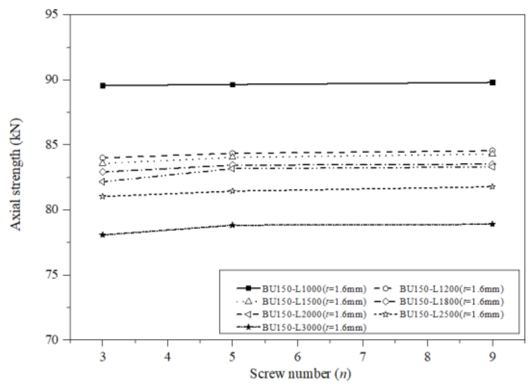

(i) BU150

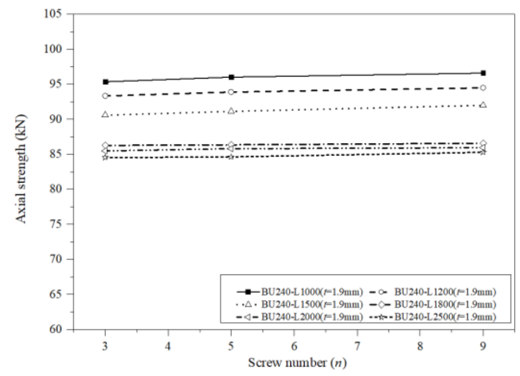

(ii) BU240

(a) Effect of screw number (n) on axial strength

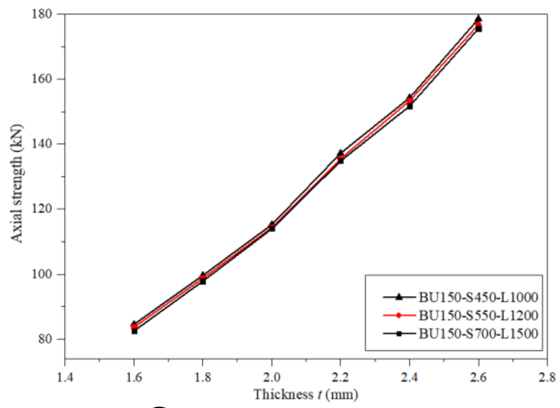

① BU150 (L=1000 to 1500mm)

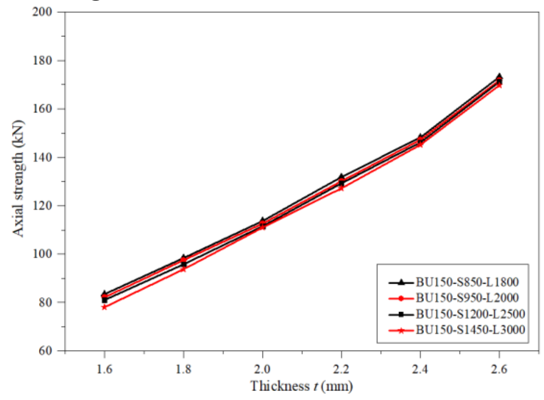

② BU150 (L=1800 to 2500mm)

(i) BU150

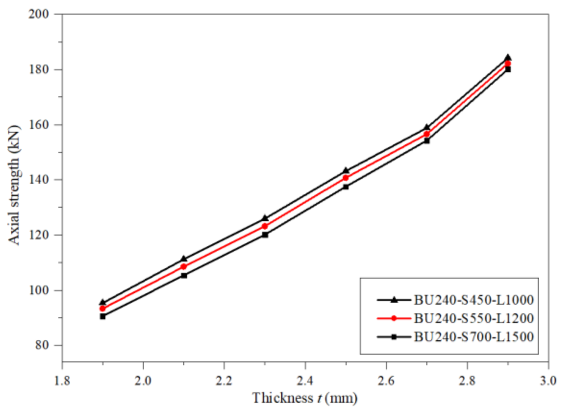

① BU240 (L=1000 to 1500mm)

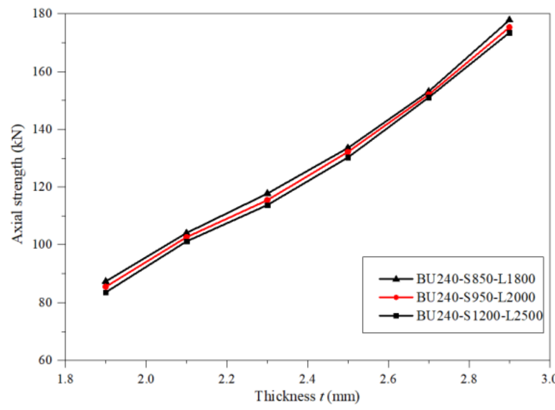

② BU240 (L=1800 to 2500mm)

(ii) BU240

(b) Effect of thickness (*t*) on axial strength

Fig.21. FE results from the parametric study

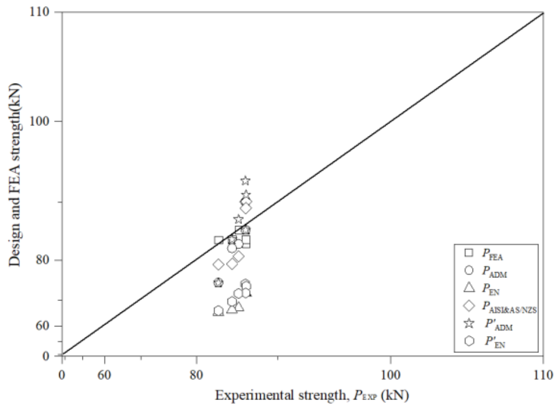

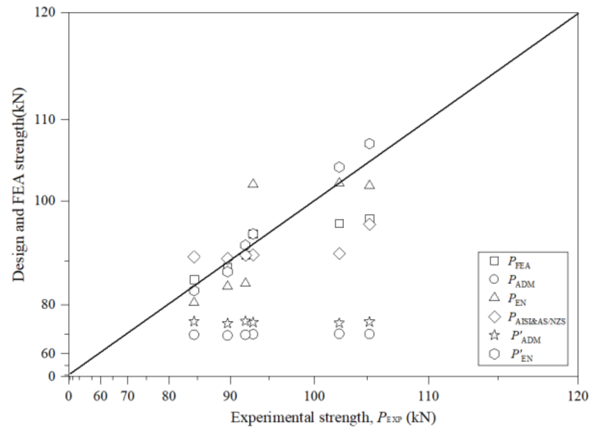

(i) BU150 (ii) BU240

(a) Comparison of axial strengths obtained from the experiments, FEA and the design standards

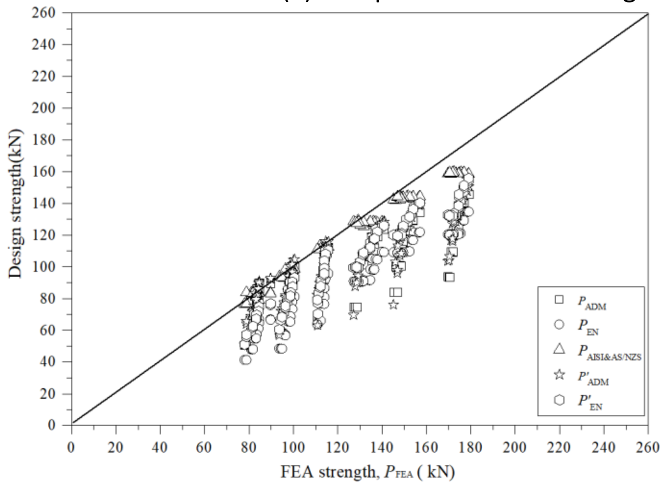

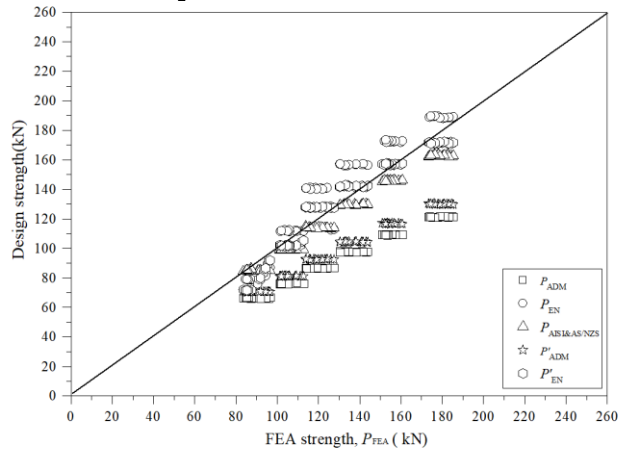

(i) BU150 (ii) BU240

(b) Comparison of axial strengths obtained from the experiments, FEA and design standards (AISI 2016&AS/NZS 2018)

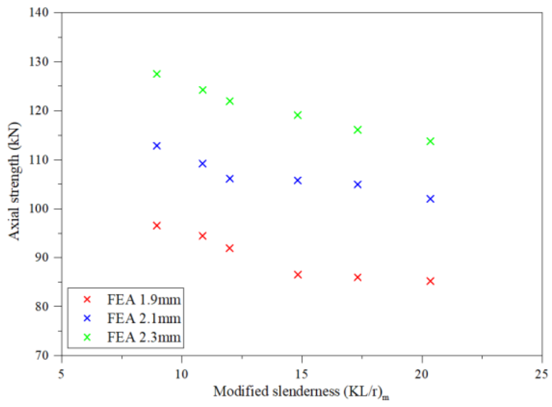

(i) Variation of strength against length for BU240 (t=1.9mm, 2.1mm,2.3mm)

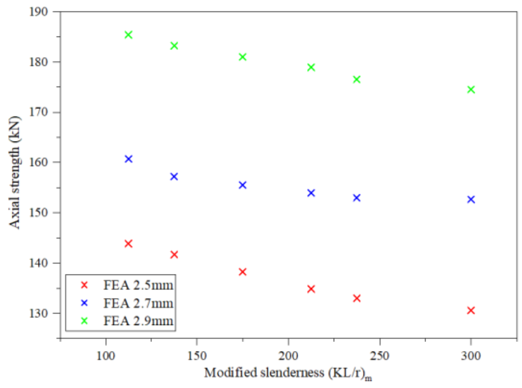

(ii)Variation of strength against length for BU240 (t=2.5mm, 2.7mm,2.9mm))

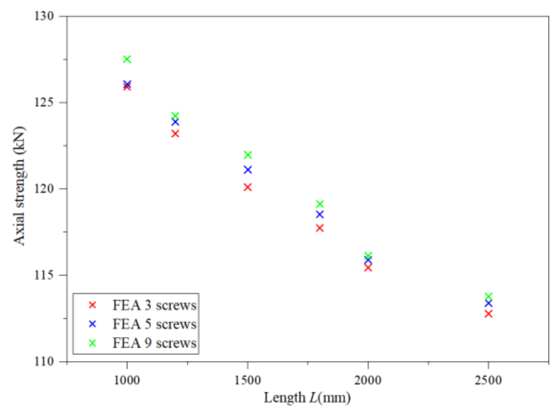

(i) Variation of axial strength against length for BU240 (t=2.30mm)

(c) Efferct of varying section thickness on column modified slenderness

(d) Effect of varying screw on axial strength

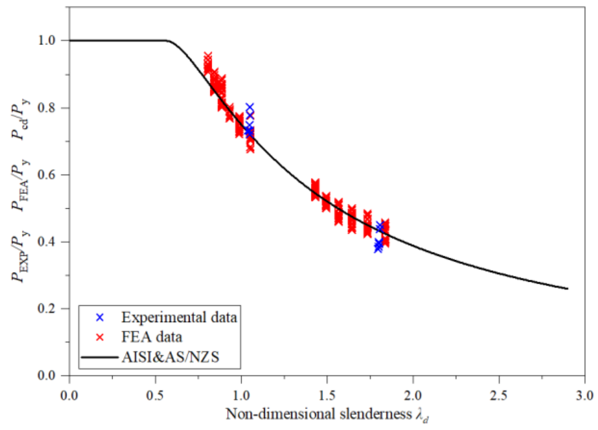

(i) Variation of axial strength against non-dimensional slenderness

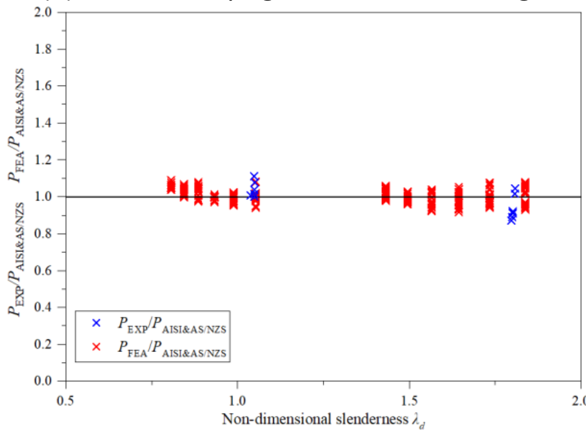

(ii) Ratio of test strength/FEA strength with design strength

(e) Comparison of test strength and FEA strength with design strength

Fig.22. Comparison of axial strength obtained from the experiments, FEA and the design standards (AISI 2016&AS/NZS 2018)